Research Square

Preprints are preliminary reports that have not undergone peer review.
They should not be considered conclusive, used to inform clinical practice,
or referenced by the media as validated information.

Agricultural liming is a large carbon sink in the Mississippi River Basin

Tim Jesper Suhrhoff

timjesper.suhrhoff@yale.edu

Yale Center for Natural Carbon Capture, Yale University

Christopher Reinhard

Georgia Institute of Technology https://orcid.org/0000-0002-2632-1027

Yoshiki Kanzaki

Georgia Institute of Technology

Samuel Shou-En Tsao

School of the Environment, Yale University

Beck Woollen

Yale University

Tom Reershemius

Newcastle Univeristy https://orcid.org/0000-0003-3512-6693

Samuel Shaheen

School of the Environment, Yale University

James Saiers

Yale University

Shuang Zhang

Texas A&M University https://orcid.org/0000-0003-1745-4642

Peter Raymond

Yale University https://orcid.org/0000-0002-8564-7860

Noah Planavsky

Yale University https://orcid.org/0000-0001-5849-8508

Physical Sciences - Article

Keywords:

Posted Date: June 19th, 2026

DOI: https://doi.org/10.21203/rs.3.rs-7068561/v1

License: This work is licensed under a Creative Commons Attribution 4.0 International License.
Read Full License

Additional Declarations: There is **NO** Competing Interest.

Version of Record: A version of this preprint was published at Nature on September 23rd, 2026. See the published version at https://doi.org/10.1038/s41586-026-11040-2.

Agricultural liming is a large carbon sink in the Mississippi River Basin

Tim Jesper Suhrhoff[1,2*], Christopher T. Reinhard[3*], Yoshiki Kanzaki[3], Samuel Shou-En Tsao[4], Beck Woollen[1], Tom Reershemius[2, 5], Samuel Shaheen[4], James Saiers[4], Shuang Zhang[6], Peter A. Raymond[4], Noah J. Planavsky[2,1*]

[1] Yale Center for Natural Carbon Capture, Yale University, New Haven, CT 06511, USA
[2] Department of Earth and Planetary Sciences, Yale University, New Haven, CT 06511, USA
[3] School of Earth & Atmospheric Sciences, Georgia Institute of Technology, Atlanta, GA 30332, USA
[4] School of the Environment, Yale University, New Haven, CT 06511, USA
[5] School of Natural and Environmental Sciences, Newcastle University, Newcastle upon Tyne, England NE1 7RU, United Kingdom
[6] Department of Oceanography, Texas A&M University, College Station, TX 77843, USA
* corresponding author: timjesper.suhrhoff@yale.edu; noah.planavsky@yale.edu; chris.reinhard@eas.gatech.edu

Abstract

The application of carbonate minerals to arable lands — agricultural liming — is a long-standing practice for counteracting soil acidification due to atmospheric pollution and anthropogenic fertilizer addition[1–3]. While this practice boosts crop yields and mitigates soil acidification[4], it is widely considered to be a significant component of agricultural emissions of carbon dioxide (CO_2)[5]. Here, we use a multi-decade timeseries of agricultural liming and anthropogenic acidity for the Mississippi River Basin — one of the largest agricultural catchments on Earth — together with results from reactive transport modeling to show that agricultural liming has acted as a net carbon sink over the last century. We show that ~75% (65-85%) of the maximum carbon dioxide removal potential of agricultural lime added since 1900 has been realized on the catchment scale, with a time lag due to soil cation exchange and solute transport of roughly ~15 years. Our results suggest that it is the addition of anthropogenic acidity to agricultural systems that should be thought of as an emissions source, rather than the addition of lime, and underscore that optimized soil pH management can significantly reduce agricultural greenhouse gas emissions while augmenting crop yields and soil health.

Main text

The agricultural sector is responsible for a significant amount of greenhouse gas (GHG) emissions, with farm-to-fork emissions comprising ~30% of total anthropogenic GHG emissions globally[6]. In the US, direct agricultural emissions account for about 10% of overall emissions and have increased by ~8% since 1990[3]. Global GHG emissions from agriculture are projected to increase approximately 30-40% by 2050[6] to meet food demands associated with human population growth. Agricultural GHG emissions are difficult to mitigate, with the agricultural sector representing a significant fraction of residual carbon dioxide (CO_2), methane (CH_4), and nitrous oxide (N_2O) emissions in net-zero scenarios from integrated assessment modeling[7–9].

A large proportion of agricultural emissions are tied to nutrient cycling and the management of soil acidity[4,10]. While essential for high crop yields, the use of nitrogen fertilizers results in lifecycle emissions of CO_2 during fertilizer production, drives soil emissions of N_2O, and acidifies soils because acidity is produced during the nitrification of ammonium (NH_4^+) to nitrate (NO_3^-) in agricultural systems[1]. Soil acidity is a major issue because it can reduce nutrient use efficiency (NUE) in crops and in extreme cases reduce crop yields because of plant aluminum toxicity[11,12]. As a result, it is often standard agronomic practice to manage soil pH through the addition of fine-grained limestone ($CaCO_3$) or dolomite ($(Ca,Mg)CO_3$) to soils, referred to here as agricultural lime. Silicates have also been used as fertilizers and to improve soil pH[13,14] and have gained recent interest as feedstocks in enhanced weathering for carbon dioxide removal (CDR)[15,16]. These practices improve yields, can improve NUE, and have been shown to reduce trace GHG emissions from many agricultural systems[4,10]. Increasing soil pH is also an incentive-based method available for reducing N_2O emissions[4,10].

However, dissolution of limestone at low pH values[17] — the conditions liming is meant to remedy — can result in the production of CO_2:

$$CaCO_3 + 2H^+ \rightarrow Ca^{2+} + CO_2 + H_2O \quad . \qquad \text{(Eq. 1)}$$

This process is the conceptual basis for the conventional assumption that agricultural liming represents a net CO_2 emissions source. For instance, the current framework used by the IPCC to evaluate country- and sector-level greenhouse gas emissions assumes that all carbon contained in

agricultural lime is emitted to the atmosphere[5], while national GHG accounting in the United States includes the assumption that roughly half of the carbon contained in agricultural lime is emitted to the atmosphere[18]. This framework presents agricultural producers and land managers with a difficult tradeoff between the positive impacts of liming on crop yield, soil health, and trace GHG emission reductions and the potential for increased agricultural CO_2 emissions.

Here, we revisit the impact of agricultural liming using multi-decade timeseries data for one of the largest agricultural watersheds on Earth — the Mississippi River Basin (MRB). We show that the current conceptual framework is inadequate for tracking the climate impacts of agricultural soil pH management. Specifically, we argue that it is the input of anthropogenic acidity to agricultural systems — sulfuric and nitric acids from fertilization and fossil fuel combustion — that drives CO_2 emissions rather than inputs of agricultural lime (see also Supplement S2). As a result, the relevant counterfactual for evaluating the impacts of agricultural liming on CO_2 fluxes is the reaction of anthropogenic acidity with natural background sources of alkalinity and inorganic carbon. We then show that 75% or more of the full CDR potential of agricultural lime application to the MRB has been realized over the last century, with a time lag between agricultural lime application and carbon export of ~15 years resulting from soil cation exchange and solute transport.

The fate of anthropogenic acidity in the Mississippi River Basin

The MRB offers the unique opportunity to assess the dynamics of acidity addition and removal through liming in agricultural lands. The catchment covers 41% of the total area — and ~2/3 of the agricultural area — of the contiguous US[19], receives the majority of agricultural lime input[1–3], and its river chemistry is heavily impacted by agricultural processes[1,20–24] (**Figure 1**). Using geospatial and timeseries data for inputs of nitrogen (N), sulfur (S)[25–30], and agricultural lime[1–3] (see Online Methods), we quantify anthropogenic acidity pollution and intentional buffering of this acidity by addition of alkalinity through agricultural liming through the last century. The records compiled here (**Figure 2**) collectively allow us to evaluate anthropogenic additions of acidity and alkalinity into the largest river system in the US during the development of industrial agriculture and the initial rise and later decline of acid pollution from fossil fuel burning.

There is a clear and well-documented increase in agricultural lime application after ~1935, from ~1 megatonne (Mt; 10^6 tonnes) of lime per year to ~20 Mt y^{-1} nationally by 1950 (**Figure 2a**). Between 1900 and 1960 the majority of agricultural lime application in the US occurred in the MRB[1–3]. Rates of fertilizer application to the MRB have also increased dramatically since 1940[31], with a significant increase between 1960-1980 to ~6 MtN y^{-1} (**Figure 2b**) and a leveling off in subsequent decades. Atmospheric acidity deposition — SO_2 and NO_x species derived primarily from anthropogenic fossil fuel combustion-— gradually increased throughout the early part of the century but have been decreasing sharply in recent decades due to air quality and emissions regulations (**Figure 2c**).

Taken together, these compiled timeseries data allow us to construct an acid-base balance for the Mississippi catchment over the last century (**Figure 2d**). Overall, anthropogenic acidity pollution increased significantly between 1900 and the 1970s, from ~0.1 terramoles of acidity (Tmol; 10^{12} mol) per year to roughly 0.5 Tmol y^{-1} by 1970. Prior to 1960 most of this acidity flux was derived from atmospheric pollution, but a sharp increase in fertilizer addition and gradual decreases in atmospheric pollution have resulted in anthropogenic fertilizer addition being the largest single source of acidity pollution since 2010. Anthropogenic acidity inputs have vastly outstripped alkalinity inputs through agricultural liming through the last century, with a nearly 15 Tmol cumulative excess of acidity input to the MRB by 2015.

Excess acidity and the carbon balance of agricultural liming

Our results indicate that inputs of alkalinity through agricultural liming in the Mississippi catchment have not been sufficient to counteract inputs of acidity from fertilizer oxidation and atmospheric pollution (**Figure 2d**). This imbalance in the acidity budget implies that soil and river pH levels are lower than they would otherwise be without human intervention. To mechanistically evaluate the impact of excess anthropogenic acidity on the carbon cycle of the Mississippi catchment we feed the acidity and alkalinity fluxes from our timeseries into a gridded reactive transport model ensemble that accounts for the effects of local soil variations in cation exchange processes, geology, and agricultural practices (see Online Methods and Supplementary Material). This allows us to attribute the fate of excess anthropogenic acidity to chemical reactions and

transport processes, allowing us to estimate the fraction of excess acidity that ultimately results in CO_2 emissions (**Figure S9**). We can then compare a "counterfactual" scenario (that includes inputs of anthropogenic acidity but without agricultural liming) to a scenario including agricultural liming based on historical data (**Figure 3a**).

Our results suggest that the potential CO_2 emissions from excess anthropogenic acidity are significantly larger than estimated CO_2 emissions from agricultural lime using the conventional IPCC and US GHG accounting frameworks (**Figure 3a**). For instance, in 1980 our results indicate that excess anthropogenic acidity was sufficient to drive CO_2 emissions equivalent to ~15 $MtCO_2$ y^{-1} with no agricultural liming, while emissions decrease to ~10 $MtCO_2$ y^{-1} with liming included. In contrast, IPCC and US GHG accounting estimates that assume agricultural lime is the source of CO_2 emissions rather than anthropogenic acidity are well below both of these values, at ~7 and 4 $MtCO_2$ y^{-1}, respectively. The current IPCC framework for calculating liming CO_2 emissions[5] only yields correct values when alkalinity addition through liming happens to match overall net-acidity inputs to the system, which has rarely been the case historically in the US (**Figure 2**) and is uncommon globally[32].

This suggests that it is the flux of anthropogenic acidity — rather than inputs of agricultural lime — that should be the metric for evaluating CO_2 emissions and constructing counterfactual scenarios for geochemical practice interventions within the agricultural system (see also Online Methods). Specifically, baseline or counterfactual rates of CO_2 emission from agricultural systems should be grounded in fluxes of anthropogenic acidity, rather than fluxes of agricultural lime, and the impact of agricultural liming on GHG emissions should be evaluated based on this counterfactual rather than based on any assumed emissions factors for lime. Indeed, our results indicate that inputs of agricultural lime in the Mississippi catchment have acted to decrease CO_2 emissions on a decadal timescale— and suggest that agricultural liming has been strongly carbon-removing at the catchment scale for most of the last century in the Mississippi watershed (**Figure 3a**).

Efficiency and timescales of carbon removal in the Mississippi River Basin

We can use the difference between the simulations with and without agricultural liming to estimate the aggregate CDR associated with liming in the Mississippi catchment over the last century (**Figure 3b**). Cumulatively, our modeling approach estimates that ~300 $MtCO_2$ have been removed through agricultural liming in the period between 1900-2015 (**Figure 3b**). We can compare this with excess riverine bicarbonate fluxes[22,23] (**Figure S1**; see Online Methods and Supplement S1) compared to a pre-1935 baseline, which indicate that an additional ~800 $MtCO_2$ has been exported cumulatively from the Mississippi catchment over the same period. Assuming this derives from the reaction of lime with carbonic acid, based on the stoichiometry of carbonate dissolution, this equates to ~400 $MtCO_2$ removed through liming and transported in the Mississippi:

$$CaCO_3 + CO_2 + H_2O \rightarrow Ca^{2+} + 2HCO_3^- \quad . \qquad \text{(Eq. 2)}$$

This correspondence between independent bottom-up (biogeochemical model-based) and top-down (river record-based) flux estimates strongly supports the contention that agricultural liming has served as a carbon removal flux in the Mississippi catchment over the last century. Consistent with this interpretation, based on changes in the ratio between Ca^{2+} and Mg^{2+} to HCO_3^- concentrations[33] (see Online Methods) our novel Mississippi River chemistry dataset (**Figure S1**) indicates that the fraction of weathering occurring due to strong acids has decreased over the same period and the catchment has gradually become a larger CO_2 sink over time (**Figure S2**).

We can evaluate the timescales and efficiency of carbon removal through agricultural liming over time by comparing the top-down (model-based) and bottom-up (river-based) flux estimates with an estimate of the total CDR potential of added lime in the Mississippi catchment assuming stoichiometric reaction of added lime with soil CO_2 (via carbonic acid; Eq.2). This approach yields a cumulative total CDR potential of lime addition amounting to ~500 $MtCO_2$ between 1900-2020, suggesting that between 65 ± 11% (model) to 85 ± 21% (river flux data) of the carbon removal potential of added lime between 1900-2015 has been realized. This is likely a conservative estimate, given that a fraction of the dissolved inorganic carbon moving through the catchment enters long-term storage in deeper groundwater[34], likely removing carbon but bypassing our river accounting. For instance, recent estimates suggest that 16% of water fluxes go toward groundwater recharge in the continental US[35] (and ~11% in the MRB). Nevertheless, we find multiple,

consistent lines of support that agricultural liming has represented a large carbon removal flux over the last century, and that on a decadal scale it is a relatively efficient carbon removal process at the catchment scale.

We can also use our timeseries and model data to evaluate the timescales over which carbon removal due to agricultural liming has unfolded relative to the time of lime application in the MRB. It is well-known that base cations released into soils (e.g., Ca^{2+} from dissolving limestone or silicates) can become bound to cation exchange sites within the soil, resulting in a time lag between cation input to the system and cation export[36–38]. Because it is the charge balance with base cations that is ultimately responsible for HCO_3^- formation and export from soil systems, any lag in cation transport will also result in a lag in carbon removal. Model results suggest that this time lag can vary considerably depending on soil properties and land use practices[39]. Our results indicate a broadly constant carbon removal lag in the Mississippi catchment of 15-30 years from the time of lime application (after 1935; **Figure 3b**). Reactive transport model results suggest that liming was a CO_2 source for the first 15 years after the initial increase in liming rates due to the release of exchangeable acidity in the soil, again highlighting the impact of cation exchange processes on CO_2 emissions and alkalinity export (supplement S1; **Figure S9**). It takes another ~15 years for this initial CO_2 pulse to be fully compensated, with model results indicating that in the MRB liming became CO_2 removing after ~30 years. These timescales are likely to vary as a function of soil conditions and agronomic practice, indicating the potential to improve the agronomic and climate impacts of liming through optimized deployment strategies and policy incentives. River based estimates show signs of less pronounced time lag in alkalinity export after the ramp up of liming **(Figure 3b)**, either due to particularly high river discharge in the 1940s or potentially suggesting the importance of regions of preferential flow in many soils.

Implications for agricultural policy and carbon removal

Much of the Mississippi catchment, like many agricultural regions, is below optimal soil pH values[40,41]. This implies that croplands are not optimized for nutrient use/retention or for yields.

Given that liming is widely accepted as a standard agronomic practice, funding and financing are likely a substantial factor contributing to the gap between ideal and realized soil pH values. Evidence that agricultural liming leads to durable carbon dioxide removal at the catchment scale — rather than being a CO_2 source — suggests that efforts to fund and incentivize management of soil pH through agricultural liming could both have positive agronomic impacts and reduce large-scale agricultural greenhouse gas emissions. This analysis also provides an impetus to focus on catchment-scale and jurisdiction-level monitoring of alkalinity fluxes as a means of robustly quantifying the enhanced weathering effects of adding carbonates and silicates to soils to modify pH values. However, if the aim of liming is to maximize carbon removal, care should be taken regarding the timescale it takes for liming to become CO_2-removing. However, our analysis suggests that agricultural liming as an agronomically beneficial mechanism of carbon removal that should be explored in croplands worldwide.

Acknowledgements

We thank R. Eugene Turner for sharing his data compilations of Mississippi River chemistry as well as for helping locate some of the earliest datapoints included in this study. TJS acknowledges funding from the Swiss National Science Foundation (P500PN_210790). TJS and NJP acknowledge funding from the Yale Center for Natural Carbon Capture and Environmental Defense Fund. CTR, JS, PAR, and NJP acknowledge funding from the US Department of Energy (DOE). CTR and NJP acknowledge funding from the Grantham Foundation for the Environment.

Author contributions

Conceptualization: TJS, NJP, CTR
Methodology: TJS, NJP, CTR
Software: TJS, YK
Validation: TJS
Formal analysis: TJS
Investigation: TJS, NJP, CTR, YK
Resources: TJS, SST
Data Curation: TJS
Writing, initial draft: TJS, NJP, CTR
Writing, review and editing: TJS, NJP, CTR, SWS, TR, SZ, JS, YK
Visualization: TJS, CTR, YK
Supervision: NJP, CTR

Project administration: TJS, NJP, CTR
Funding acquisition: TJS, NJP, CTR

Figures

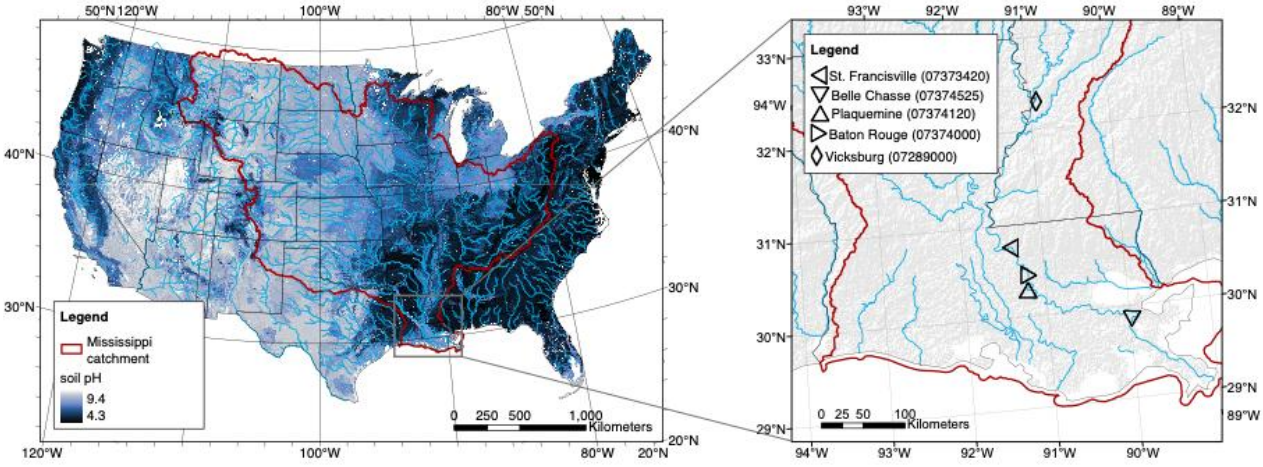


Figure 1: Timeseries domain for the Mississippi River Basin (MRB). Shown in (***a***) is the region considered in our timeseries analysis, with soil pH values for areas with >10% cropland shown for context. Shown in (***b***) is a regional map of the USGS river gauging stations used in this study to construct downstream timeseries of riverine fluxes (see **Figure S1**).

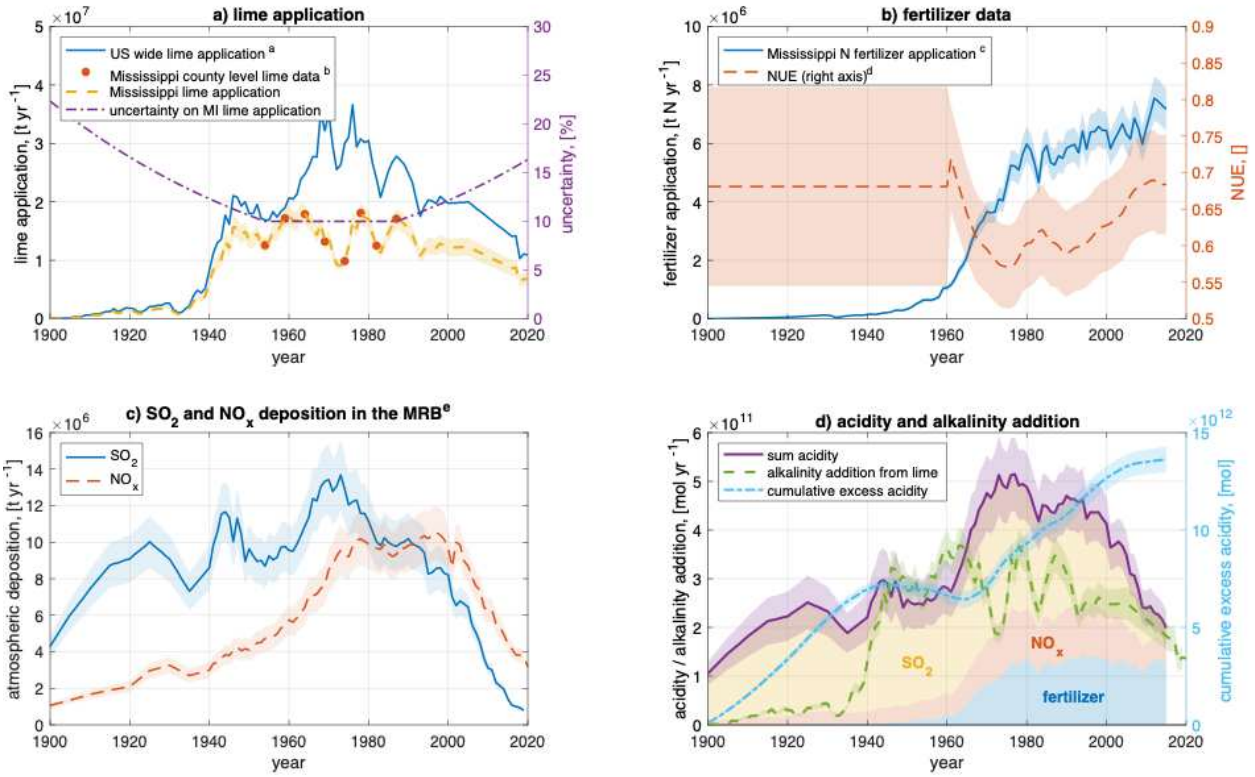


Figure 2*:* Reconstructed timeseries data for US-wide[1,3] and Mississippi catchment lime application rates (***a***), annual fertilizer application rates[31] and nitrogen use efficiency (NUE[42]) (***b***), atmospheric SO_2 and NO_x deposition fluxes[25–30] (***c***), and combined acid-base budget (***d***) for the MRB. NUE values prior to start of timeseries data in (***b***) are assumed constant. All uncertainties shown correspond to 1 standard deviation. Uncertainty on cumulative excess acidity is based on Monte Carlo simulations assuming a minimum uncertainty of 10%.

[a] West & McBride (2007) and EPA (2022) [1,3] [b] U.S. Bureau of Census (1956-1989) [2] [c] Cao et al. (2017)[31] [d] Zhang et al. (2015)[42] [e] based on data from Turner (2021) and U.S. Bureau of Census (2003) [28–30] as well as combined model and observation data for atmospheric deposition[25–27]

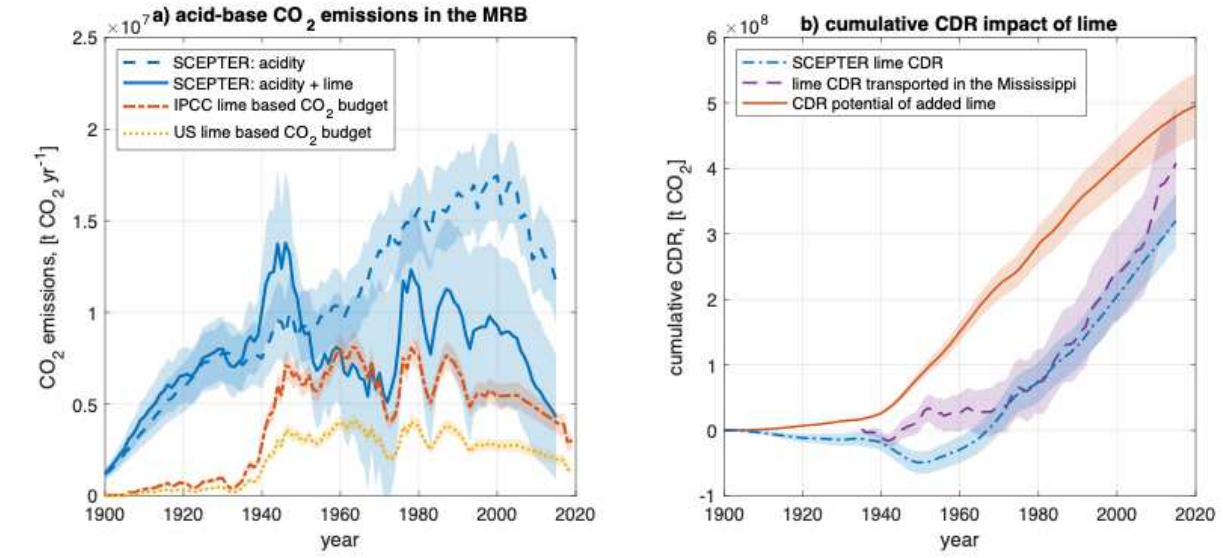


Figure 3: Comparison of agricultural CO_2 budgets estimated based on reactive transport modeling and river gauging data. Shown in (***a***) are CO_2 emissions based on our reactive transport model driven by the timeseries data for anthropogenic acidity flux with (blue-solid) and without (blue-dashed) agricultural liming. Also shown for comparison are estimated CO_2 emissions using the IPCC (red-dashed) and US-GHG (yellow-dotted) frameworks for estimating lime-derived CO_2 fluxes. Shown in (***b***) are estimates of cumulative carbon dioxide removal (CDR) based on complete reaction with soil CO_2 (red-solid), CO_2 captured relative to the no-lime counterfactual in the reactive transport model (blue-dash-dotted), and bicarbonate excess in river data for the Mississippi catchment (purple-dashed).

Online Methods

In this project we combine long timeseries of cation and bicarbonate concentrations in the Mississippi River watershed with records of lime and acidity addition to re-visit the question whether liming in the Mississippi watershed is CO_2 sink or source[1,33] and argue that emissions should be attributed to acidity additions rather than liming itself and attempt to estimate agricultural CO_2 budgets based on this assumption.

To compile these data, riverine concentrations and fluxes are estimated by combining long timeseries of Ca and Mg concentrations from 5 USGS stations in the Lower Mississippi River[43], and of previously published records of discharge and alkalinity [22,23]. Using the approach outlined in Hamilton et al. (2007)[33], we quantify the fraction of carbonate weathering that occurs because of reactions with strong (i.e., non-carbonic) acid based on the concentrations of Ca, Mg, and bicarbonate. For the part of the time series where cation data is lacking (1901-1953), the strong acid fraction is estimated by modulating the linear interpolation with changes in acidity pollution considering oxidation of fertilizer, and NO_x and SO_2 emissions as sources of acidity. Given the strong correlation of SO_2 emissions with coal production before 1955 (**Figure S10**), by modulating the trend with SO_2 we assume to also capture changes in acid mine drainage from coal mining. Estimates of the former are based on data on fertilizer addition[31] and nitrogen use efficiency[42], while atmospheric acidity pollution relies on emission[28–30] as well as atmospheric deposition data [25–27]. Based on reactive transport model derived [39,44,45] estimates of the fraction of acidity reacting with bicarbonate to produce CO_2, we further compare how different approaches of attributing CO_2 emissions deriving from the reaction of strong acids with bicarbonate or lime translate into agricultural CO_2 budgets. In this section we are giving detailed information on how the parameters presented in this study are derived and calculated.

Annual average riverine concentrations in the Lower Mississippi

The MRB data analyzed here build upon concentration measurements from 5 USGS stations[43] (**Figure 1**, **Figure S1**) spanning 7 decades, as well as published data from the early

1900s[46,47] and long timeseries of Mississippi discharge and total alkalinity titrations (assumed to be equivalent with HCO_3^- concentrations)[22,23]. All data compiled in this study as well as calculated results are available in the data supplement.

Annual flow weighted average concentrations for Ca (combining USGS parameters 00915 and 00916), Mg (00925 and 00927), SO_4^{2-} (00945) and NO_3^-+NO_2^- (00631) were calculated based on the data of from the following stations (see **Figure 1**):

- Mississippi River at Vicksburg, MS – station 07289000
- Mississippi River at St. Francisville, LA – station 07373420
- Mississippi River at Baton Rouge, LA – station 07374000
- Mississippi River at Plaquemine, LA – station 07374120
- Mississippi River at Belle Chasse, LA – station 07374525

Due to their similar watersheds and to maximize the amount of data per year and month, data from these 5 stations were combined and monthly average concentrations were calculated. Using monthly discharge data[22], annual flow weighted averages were calculated. The uncertainties from monthly averages were propagated assuming a 10% uncertainty on monthly discharge and the calculated standard deviation on monthly average concentrations. Uncertainties on both monthly average and annual flow weighted average concentrations were set to be 5% when propagated uncertainties were lower. Annual fluxes were calculated by combining annual flow weighted average concentrations with annual water discharge[22,23]. Uncertainties were propagated assuming 10% uncertainty on annual discharge. The calculated annual average concentrations are shown in **Figure S1** and briefly discussed in Supplement S1.

To estimate the increase of riverine bicarbonate fluxes compared to the pre-lime baseline period, we calculate the average pre-1935 bicarbonate concentrations (baseline) and the excess over this baseline for the post 1934 period. Uncertainties on the baseline value, excess riverine bicarbonate fluxes as well as their cumulative value are propagated using Monte Carlo simulations. Estimates of excess riverine bicarbonate fluxes in terms of lime CDR are calculated based on the assumption that the excess flux is caused by dissolution of lime, half of the related C stems from the atmosphere and half from lime minerals. Riverine transported lime-CDR is hence estimated by converting 50% of excess (molar) bicarbonate fluxes into metric tons of CO_2.

Fraction strong acid weathering

Our approach to quantify the fraction of lime dissolved as a result of reaction with strong acids rather than carbonic acid builds upon the classic approach of comparing water Ca and Mg concentrations (in meq/L) with water HCO_3^- concentrations (in meq/L) as developed by Hamilton et al. (2007)[33] – see also **Figure 4**. Historically, this approach was applied to tile drainage and stream water[33]. Here, we assume that this framework also applies to the Mississippi watershed for three reasons. First, ~58% of the catchment is covered with croplands[48] and overall riverine processes are heavily impacted by agriculture[1,20–24], facilitating the emergence of an agricultural liming signal. Second, weathering fluxes in the Mississippi catchment are generally dominated by carbonate weathering[49], such that this framework would be expected to reflect carbonate weathering dynamics also on the catchment scale.

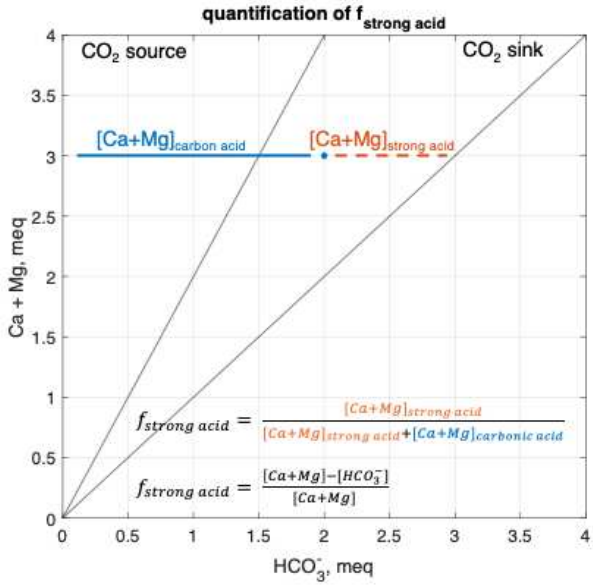


Figure 4: Sketch of the quantification of the fraction strong acid weathering ($f_{strong\ acid}$) from Ca, Mg, and HCO_3^- concentrations.

Essentially, lime dissolution by carbonic acid releases Ca+Mg and HCO_3^- at a 1:1 ratio (in meq/L). If strong acids are present and react with lime, this releases cations without generating HCO_3^-. Stoichiometrically, this is equivalent with dissolution via carbonic acid, and subsequent loss of

HCO_3^- due to reaction with protons are charge balanced by strong acids. Hence, we quantify the fraction strong acid $f_{strong\ acid}$ weathering as a unitless ratio:

$$f_{strong\ acid}[] = \frac{[Ca+Mg]_{strong\ acid}}{[Ca+Mg]_{strong\ acid}+[Ca+Mg]_{carbonic\ acid}} \quad \text{(eq. 3)}$$

Where $[Ca+Mg]_{strong\ acid}$ and $[Ca+Mg]_{carbonic\ acid}$ are the concentrations of Ca+Mg (in meq/L) released by the reaction of lime with strong acids and carbonic acid, respectively. The sum of these two simply is the concentration (in meq/L) of Ca+Mg in water.

$$[Ca+Mg] = [Ca+Mg]_{strong\ acid} + [Ca+Mg]_{carbonic\ acid} \quad \text{(eq. 4)}$$

Because the concentration of HCO_3^- is equivalent to the cations released from carbonic acid weathering (on a charge balance basis) we can rewrite this equation and solve for $[Ca+Mg]_{strong\ acid}$:

$$[Ca+Mg] = [Ca+Mg]_{strong\ acid} + [HCO_3^-] \quad \text{(eq. 5)}$$

$$[Ca+Mg]_{strong\ acid} = [Ca+Mg] - [HCO_3^-] \quad \text{(eq. 6)}$$

Substituting equations 4 and 6 into 3, we can calculate the fraction strong acid weathering as a function of measured quantities:

$$f_{strong\ acid} = \frac{[Ca+Mg]-[HCO_3^-]}{[Ca+Mg]} \quad \text{(eq. 7)}$$

We calculate $f_{strong\ acid}$ for the period where data is available: for all years after 1954 and for 1900 based on alkalinity data for 1900[22,23] and cation concentrations for 1901[47], assuming these data can be grouped to calculate one valid data point for 1900 based on the data of two years. To constrain processes in the period 1901-1953, we estimate how $f_{strong\ acid}$ developed based on the interpolation between the years 1900 and 1953 as well as changes in acidity generating processes in that period. The two acidity generating processes considered are the oxidation of fertilizer and environmental pollution with sulfuric and nitric acid (see relevant sections below for more detail).

The two signals used to modulate the linear interpolation are the annual acidity generation from fertilizer oxidation and the annual acidity generation from SO_2 and NO_x emissions (**Figure 2d**). To modulate the $f_{strong\ acid}$ interpolation, we linearly interpolate for the summed acidity generation of both processes. For each year we calculate a modulation factor which is the ratio between the actual data for that year and the linear interpolation. The signal is primarily dominated by atmospheric acid pollution, consistent with low fertilizer addition rates prior to that year (**Figure 2b**).

In addition to calculating $f_{strong\ acid}$, this approach also allows calculating the cations released by strong acid weathering, irrespective if initial weathering occurred due to reaction with carbonic acid and subsequent reaction of bicarbonate with protons from strong acids (equation 7).

Rather than using $f_{strong\ acid}$, Hamilton et al. (2007)[33] discuss lime dissolution processes in terms of "CO_2-C sink strength":

$$CO_2 - C\ sink\ strength\ (\%) = \frac{([HCO_3^-] - 0.5[Ca+Mg])}{0.5[Ca+Mg]} * 100 \quad \text{(eq. 8)}$$

The two terms are related in that a $f_{strong\ acid}$ value of 0.5 corresponds to a $CO_2 - C\ sink\ strength$ of 0%, and $f_{strong\ acid}$ values below 0.5 correspond to negative $CO_2 - C\ sink\ strength$ values (with $f_{strong\ acid}$ (0) = $CO_2 - C\ sink\ strength$ (-100%)) and $f_{strong\ acid}$ values above 0.5 correspond to positive $CO_2 - C\ sink\ strength$ values (with $f_{strong\ acid}$ (1) = $CO_2 - C\ sink\ strength$(100%)). Hence, all data pairs that fall to the left of the line with the slope 2 are considered CO_2 sources and all data points to the right CO_2 sinks. This is because the assumption is that on timescales shorter than that of carbonate precipitation in the oceans, half of the carbon in the HCO_3^- released via the reaction of lime with carbonic acid derives from the atmosphere and that this can be considered a CO_2 sink. Hence, if less than half of HCO_3^- is lost due to reaction with strong acids and subsequent degassing ($f_{strong\ acid}$ < 0.5, $C\ sink\ strength$ of 0-100%), this process constitutes a CO_2 sink on this timeframe. If more than half of the bicarbonate reacts with strong acids to produce CO_2, lime dissolution is an overall CO_2 source ($f_{strong\ acid}$ > 0.5, $C\ sink\ strength$ of -100-0%).

How $f_{strong\ acid}$ and $C\ sink\ strength$ evolve through time based on the records compiled here is presented **Figure S2** in and discussed in supplement S1. Cumulatively, river data indicates that driven by reductions in strong acid input, the MRB has become a stronger CO_2 sink.

Liming data and uncertainties

To estimate lime application in the Mississippi watershed, we combine US-wide liming data[1,3] from 1900-2020 with county level data[2] from 1954-1987 to estimate lime addition to the Mississippi watershed for the whole period. Lime application in the Mississippi watershed is calculated for the years 1954, 1959, 1964, 1969, 1974, 1978, 1982, 1987 by summing application data for all counties contained within the Mississippi watershed from county level data [2]. For counties that are partially within the watershed, the total amount applied is scaled down by the area of the county contained within the Mississippi watershed. Between the years where county level data is available, county level data is interpolated, and the interpolation is modulated with the signal of the US-wide data[1,3]. Unfortunately, no county level liming data is available outside the period 1954-1987. After 1987, lime application was grouped with fertilizer in Census reports. Because this sum is reported in mass and different types of fertilizer have different nitrogen to mass ratios, deconvolving the reported sum into its constituents lime and fertilizer application is non-trivial and not attempted here. Outside this period, we estimate Mississippi wide lime application by scaling the US wide application data down assuming the fraction of lime applied within the Mississippi watershed remained constant (constant at 1954 proportion before 1954 and constant at 1987 proportion after 1987). To account for the fact that moving away from the 1954-1987 period the data is less constrained with county level deployment data, we increase the assumed uncertainty on Mississippi lime application rates: it is set to 10% for 1954-1987, and increases by 1.5 % for each year moving away from this period, resulting in a ~22% uncertainty in 1900 and ~16% uncertainty in 2020 (**Figure 1a**).

Mass application rates were converted to molar amounts by taking into account relative contributions of "quicklime and hydrated lime" and "crushed limestone and dolomite", while assuming the latter is composed of 20% dolomite and 80% limestone[1].

Acidity generation from fertilizer oxidation

This study assesses the release of fertilizer as well as NO_x and SO_2 emissions derived acidity for three primary reasons. First, to estimate the fraction of strong acid weathering for the part of the record where cation data is lacking. Second, to assess to what extent liming as balances the addition of acidity in the Mississippi Catchment. And third, to relate acidity generation to related CO_2 emissions in the context of attributing emissions deriving from the reaction of lime/bicarbonate with strong acids to lime application or acidity addition. The acid sources considered are the oxidation of nitrogen fertilizer as well as NO_x and SO_2 pollution.

Nitrogen can be supplied to fields in either reduced or oxidized form, and once added these compounds react in various ways as part of the natural N cycle, with some of these processes acting as a net source of acidity to the agricultural system. To assess related elemental and acidity fluxes on the Mississippi catchment scale, here we adopt a simplified conceptual model of the N cycle (**Figure S11**), which nevertheless is consistent with previous work that has assessed the impact of modifying soil acid-base balances via enhanced rock weathering[50]. This analysis is based on several assumptions:

1. Assuming that, due to fast nitrification reactions[51,52], ammonia (NH_4) is nitrified to NO_3^- before it is taken up by plants, N added via fertilizer produces 1 mol H^+ per mol of N. Fertilizers usually contain a significant amount of NH_4 producing substances[31], such as Urea or anhydrous ammonia (NH_3). The reaction of these to NH_4 consumes 1 mol H^+ per mol of N. Subsequently, in a process called nitrification, NH_4 is oxidized in a two-step reaction to nitrite (NO_2^-, by Nitrosomonas bacteria), and then to nitrate (NO_3^-, by Nitrobacter bacteria), releasing 2 mol of H^+ per mol ammonia, such that overall 1 mol H^+ is produced per

mol N added (NO_3^-). This is also true for fertilizer added as ammonium nitrate (NH_4NO_3), where the nitrification of ammonia releases 2 H^+ (for two N).

2. Only the nitrate that remains in solution and is ultimately leached from soils remains charge balanced by H^+, while the rest of the reactions including plant uptake and denitrification consumes the initial acidity (**Figure S11**).

Hence, the acidity produced from fertilizer addition is calculated from the molar amount of N added after taking into account the fraction of N taken up by plants as well as denitrification/degassing:

$$fertilizer\ acidity\ production\ [mol\ H^+/yr] = \frac{fertilizer\ N\ application\ [g/yr]}{M_N} * (1 - NUE) * f_{NO_3^-,leached} \quad \text{(eq. 9)}$$

where $fertilizer\ application$ is the annual nitrogen fertilizer addition flux (g N/yr), M_N the molar mass of N (g/mol), NUE is the nitrogen use efficiency (dimensionless; 1 - NUE as to quantify the fraction lost rather than used), and $f_{NO_3^-,leached}$ is the fraction of the remaining N (i.e., the N not taken up by plants) that is leached and not lost to the atmosphere.

The primary data used for this analysis is spatially explicit nitrogen fertilizer addition timeseries data[31]. For each year from 1900 to 2015, the average nitrogen fertilizer addition for the Mississippi catchment was calculated using ArcGIS (i.e., clipping the Mississippi catchment area and calculating the average value) and transferred into a mass flux based on the Mississippi catchment area. These data are model-based, but compare well with other estimates of nitrogen fertilizer addition[31,53,54]. Assumed uncertainties on the nitrogen fertilizer application rates are 10% for every year. Nitrogen use efficiency for the time series is based on published data from 1961-2012[42] and assuming NUE were constant at the 1961-1965 average value before 1965. Due to low nitrogen fertilizer use before 1960, the impact of this parameter on the propagated overall cumulative acidity production in the period before 1960 is low. Uncertainty on NUE was assumed to be 10% after 1960 and 20% before 1960. Based on a global analysis, we assume that on average, 80% of the nitrate not taken up by plants is ultimately leached and remains charge balanced by H^+ (i.e., $f_{NO_3^-,leached}$)[55], and assume and propagate an uncertainty of 20% on this process to reflect the natural uncertainty and variability of related processes.

Atmospheric acidity pollution

Because it is not trivial to relate (changes in) riverine SO_4^{2-} and NO_3^- fluxes to acid pollution, we attempt to quantify these processes "top down", similarly to the quantification of acidity production from fertilizer. Similarly, although data for coal production[56], impacts of acid mine drainage on river chemistry[57], etc., exist, it is difficult to convert them into acidity production fluxes. Hence, here we estimate sulfuric and nitric acid additions to the MRB based on emission data[28–30]. For sulfuric acid pollution, we are assuming that the oxidation of 1 mol of SO_2 produces 2 mol H^+, and that similarly to NO_3^-, plant uptake consumes acidity through charge balance:

$$sulfuric\ acid\ pollution\ [mol\ H^+/yr] = SO_2\ emissions[mol/yr] * f_{SO_2-Mississippi} * 2 * f_{SO_4^{2-},leached} \quad \text{(eq. 10)}$$

where $f_{SO_2-Mississippi}$ is the fraction of US wide SO_2 pollution occurring within Mississippi catchment and was calculated (**Figure S12**) based on "Total Deposition Science Committee" TDep data which integrates observations of atmospheric concentrations (CASTNET, NTN, MDN) with an atmospheric model (CMAQ) to estimate deposition of numerous pollutants within the US[25–27]. The fraction was calculated for the years 2000-2021 where data is available, and the average of these years (0.430 ± 0.023) is used for the earlier part of the time series (1900-1999) assuming that this fraction has remained constant. The fraction is calculated based on TDep parameter so2_dw (dry deposition of SO_2), but the result using s_tw (dry + wet deposition of S compounds) is the same within error (0.429 ± 0.017). These values are also similar compared to the area fraction of the contiguous US that is within the Mississippi catchment: 41%[19]. Although the calculated uncertainty is lower, we assume an uncertainty of 10% on $f_{SO_2-Mississippi}$ for the pre-2000 data, as do we assume an uncertainty of 10% on SO_2 emission data and propagate the uncertainties on the production of sulfuric acid as a result of SO_2 pollution. Sulfate leaching in soils is highly variable and depends on a whole range of factors[58–60], hence assuming a static value here (as for the other parameters) necessarily represents a first order estimation. Based on experimental data using sulfate fertilizer, here we use a leaching rate of 72%[59], assuming that this fraction remains charge balanced by H^+. We propagate an uncertainty of 20% on this estimate to reflect natural variability and the uncertainty on the catchment-level average.

Parameterizing environmental pollution with sulfuric acid in terms of SO_2 emissions means assuming that atmospheric deposition of SO_2/SO_4^{2-} is the primary source of sulfuric acid pollution rather than direct runoff from acid mine drainage. Although catchments that are highly impacted by coal mining likely see more pollution from direct runoff[57], on the scale of the whole Mississippi catchment, where most areas are not affected by coal mining, this assumption is likely valid to a first degree. Generally, as SO_2 emissions are primarily derived from coal burning[61,62], in the early part of the record before that is relevant for the interpolation of $f_{strong\ acid}$, trends in SO_2 emissions should also capture dynamics in coal mining and therefore acid mine drainage (**Figure S10**).

Acidity addition from NO_x pollution is based on emissions data [3,29] which is transferred from a mass to a molar flux using a NO fraction of 0.050 based on Nitrogen Dioxide/Nitrogen Oxide In-Stack Ratio (ISR) Database[63] (i.e., assuming that NO_x is composed to 5% out of NO and 95% NO_2). As for SO_2, deposition occurring in the Mississippi catchment was calculated (**Figure S12**) based on TDep data [25–27] for the years with data and assumed to be constant before this period. One NO_x-N is assumed to produce one NO_3^- charge balanced by H^+, and the fraction that remains charge balances is propagated through the simplified N cycle as done for fertilizer (equation 9).

The way we calculate acidity addition is designed to yield a first order estimate, representative at the catchment scale. Clearly there is a lot of variability in related processes, particularly the fractions of N and S that are taken up by plants vs. leached – but overall we take this into account by using conservative, generous estimates of uncertainty on all parameters used as inputs in this study.

Assessing the fate of acidity using the reactive transport model SCEPTER

Translating acidity addition to agricultural fields into related CO_2 emissions requires estimating what fraction of protons reacts with bicarbonate to produce carbonic acid which may ultimately degas as CO_2, and what fraction exchanges with base cations on cation exchange sites. For this we utilize the reactive transport model SCEPTER[39,44,45], which has recently been used to

561 track the lag times associated with alkalinity additions in the soils of the US[39]. We assess the
562 impact of lime on CO_2 emissions from acid neutralization reactions (and reductions thereof) by
563 comparing SCEPTER simulations with acidity and alkalinity inputs to the counterfactual scenario
564 in the absence of lime addition: acidity addition only.
565
566 SPECTER is spun up for 1°x1°C grid cells for the US where cropland constitutes at least
567 10% of areal extent [64] considering a soil depth of 0.5m. The initial and spin-up boundary conditions
568 for the reactive transport code are based on a variety of gridded data products, including
569 runoff/infiltration[35], mean annual air temperature[65], aboveground net primary productivity
570 (NPP)[66], soil organic matter (SOM)[67], topsoil pH[67], soil cation exchange capacity (CEC)[68], and
571 soil base saturation[67]. SCEPTER is initialized by tuning four key parameters:
572 1. a reference soil cation exchange coefficient ($K_{H/Na}$)[64]
573 2. dissolved Ca^{2+} concentration at the upper boundary
574 3. input of soil organic carbon (J_{org})
575 4. soil organic carbon (SOC) turnover time (τ_{org}).
576 These parameters are adjusted to reproduce four site-specific observational parameters: soil pH,
577 soil base saturation, soil organic carbon content, and soil pCO_2, which is estimated from soil
578 temperature and net primary productivity[69]. The model is forced by other boundary conditions,
579 such as runoff and air temperature. Before start of the simulations, the model is spun up for 10^5 yr
580 to ensure processes are initially at steady state.
581
582 For the experiments conducted here, the quantities of acid forming pollution and fertilizer
583 (i.e., the fluxes assumed to remain charge balanced by protons in contrast to acidity neutral
584 pathways; **Figure S11**) are fed into the model as H_2SO_4 for SO_2 pollution, and as NH_4NO_3 for
585 HNO_3 production from fertilizer and NO_x pollution (based on equations 9 and 10, converted to
586 mg/m^2/yr). Lime alkalinity is introduced into the model as 80% of calcite and 20% of dolomite[1].
587 These fluxes are modulated to reflect the evolution of alkalinity and acidity addition to the
588 Mississippi catchment, with atmospheric acidity pollution being normalized to the catchment area
589 of the whole catchment and lime and fertilizer addition to the agricultural area assuming that the
590 catchment is covered to 58% by agricultural land[48] to yield input fluxes representative of the
591 Mississippi average (**Figure S7**). The counterfactual scenario model runs (i.e., what would

emissions have looked like without the addition of lime) consider only the abovementioned acidity inputs.

The model is run for 116 years (assumed to correspond to the years 1900-2015), and the fractions of H^+ that exchange with base cations on exchangeable sites ($f_{H,exch}$) as well as that react with bicarbonate to produce CO_2 are calculated for each grid cell. The latter quantity is calculated using two approaches. First, based on mass balance, assuming that the amount of H^+ that for a given timestep neither enters the exchangeable pool, nor advects out of the soil column, nor is in soil pore waters reacts with bicarbonate (H_{rxn}):

$$H_{rxn} = H_{diss} - (H_{exch} + H_{adv} + H_{exch}) \quad (9)$$

Where H_{diss} is the acidity of dissolved substances after initial reaction of lime with protons to produce bicarbonate and dissolved cations (see supplement S3 for more detail). The second approach is to calculate the fraction from the flux of CO_2 diffusing to the atmosphere (H_{diff}), with both approaches leading to consistent results (<5% difference). These fluxes are normalized to the input of acidity at each timestep to give the fraction of H^+ that reacts with bicarbonate to produce CO_2 ($f_{H,rxn}$, $f_{H,diff}$). These fractions are calculated for each grid cell for each immediate timestep as well as the cumulative average since beginning of the experiments. Finally, consistent with utilizing Mississippi scale average inputs, we calculate the average of these fractions for the whole Mississippi catchment to facilitate the assessment of average acid-base processes on the catchment scale. This average fraction of acidity reacting with bicarbonate ($f_{H,rxn}$) is multiplied with the gross (or legacy) CO_2 emission potential of the added acidity (assuming 1 proton causes degassing of 1 CO_2 molecule) to calculate the flux that is realized on the short term.

More detail on SCEPTER can be found elsewhere[39,44,45], and additional analysis of model set up and output is included in the supplementary material.

References

1. West, T. O. & McBride, A. C. The contribution of agricultural lime to carbon dioxide emissions in the United States: Dissolution, transport, and net emissions. *Agric Ecosyst Environ* **108**, 145–154 (2005).
2. U.S. Bureau of Census. *Census of Agriculture: 1954*. (US Government Printing Office, Washington, DC, 1956).
3. EPA. *Inventory of U.S. Greenhouse Gas Emissions and Sinks: 1990-2022*. *EPA 430-R-24-004* (U.S. Environmental Protection Agency, 2024).
4. Wang, Y. *et al.* Potential benefits of liming to acid soils on climate change mitigation and food security. *Glob Chang Biol* **27**, 2807–2821 (2021).
5. De Klein, C. *et al.* Chapter 11 - N2O Emissions from managed Soils and CO2 Emissions From Lime and Urea Application. in *IPCC Guidelines for National Greenhouse Gas Inventories Volume 4: Agriculture, Forestry and Other Land Use* 11.1-11.54 (IPCC, 2006).
6. IPCC. Technical Summary. in *Climate Change and Land: an IPCC special report on climate change, desertification, land degradation, sustainable land management, food security, and greenhouse gas fluxes in terrestrial ecosystems* (eds. Shukla, P. R. et al.) 35–74 (2019).
7. Buck, H. J., Carton, W., Lund, J. F. & Markusson, N. Why residual emissions matter right now. *Nat Clim Chang* **13**, 351–358 (2023).
8. Lamb, W. F. The size and composition of residual emissions in integrated assessment scenarios at net-zero CO2. *Environmental Research Letters* **19**, (2024).
9. IPCC. *Assessment Report 6 Climate Change 2021: The Physical Science Basis*. (Cambridge University Press, Cambridge, United Kingdom and New York, NY, USA, 2021). doi:10.1017/9781009157896.001.
10. Zhang, H. M. *et al.* Liming modifies greenhouse gas fluxes from soils: A meta-analysis of biological drivers. *Agric Ecosyst Environ* **340**, 108182 (2022).
11. Baligar, V. C., Fageria, N. K. & He, Z. L. Nutrient use efficiency in plants. *Commun Soil Sci Plant Anal* **32**, 921–950 (2001).
12. Ur Rahman, S. *et al.* Aluminum phytotoxicity in acidic environments: A comprehensive review of plant tolerance and adaptation strategies. *Ecotoxicol Environ Saf* **269**, 115791 (2024).
13. Swoboda, P., Döring, T. F. & Hamer, M. Remineralizing soils? The agricultural usage of silicate rock powders: A review. *Science of the Total Environment* **807**, 150976 (2022).
14. Hensel, J. *Bread from Stones: New and Rational System of Land Fertilization and Physical Regeneration*. (1894).
15. Beerling, D. J. *et al.* Potential for large-scale CO2 removal via enhanced rock weathering with croplands. *Nature* **583**, 242–248 (2020).
16. Hartmann, J. *et al.* Enhanced chemical weathering as a geoengineering strategy to reduce atmospheric carbon dioxide, supply nutrients, and mitigate ocean acidification. *Reviews of Geophysics* **51**, 113–149 (2013).
17. Dietzen, C. & Rosing, M. T. Quantification of CO2 uptake by enhanced weathering of silicate minerals applied to acidic soils. *International Journal of Greenhouse Gas Control* **125**, 103872 (2023).

18. Ogle, S. M. *et al.* Quantifying Greenhouse Gas Sources and Sinks in Cropland and Grazing Land Systems. in *Quantifying greenhouse gas fluxes in agriculture and forestry: Methods for entity-scale inventory* (eds. Hanson, W. L. & Edquist, K.) 1–133 (U.S. Department of Agriculture, Office of the Chief Economist, Washington, DC, 2024).
19. Kolpin, D. Importance of the Mississippi River Basin for investigating agricultural-chemical contamination of the hydrologic cycle. *Science of the Total Environment* **248**, 71–72 (2000).
20. Oh, N. H. & Raymond, P. A. Contribution of agricultural liming to riverine bicarbonate export and CO2 sequestration in the Ohio River basin. *Global Biogeochem Cycles* **20**, 1–17 (2006).
21. Raymond, P. A. & Cole, J. J. Increase in the export of alkalinity from North America's largest river. *Science (1979)* **301**, 88–91 (2003).
22. Raymond, P. A. & Hamilton, S. K. Anthropogenic influences on riverine fluxes of dissolved inorganic carbon to the oceans. *Limnol Oceanogr Lett* **3**, 143–155 (2018).
23. Raymond, P. A., Oh, N. H., Turner, R. E. & Broussard, W. Anthropogenically enhanced fluxes of water and carbon from the Mississippi River. *Nature* **451**, 449–452 (2008).
24. Turner, R. E. Water quality at the end of the Mississippi River for 120 years: the agricultural imperative. *Hydrobiologia* (2023) doi:10.1007/s10750-023-05383-4.
25. Schwede, D. B. & Lear, G. G. A novel hybrid approach for estimating total deposition in the United States. *Atmos Environ* **92**, 207–220 (2014).
26. Beachley, G. *et al.* Improved Total Deposition Measurement Model Fusion (Tdep Mmf) Application and Evaluation of U.S. Total Atmospheric Deposition Estimates. *SSRN* (2024) doi:10.2139/ssrn.4852968.
27. NADP. Total Deposition Estimates Using the Measurement Model Fusion (TDep MMF version 2022. 02) Approach with Modeled and Monitoring Data. *National Atmospheric Deposition Program* https://gaftp.epa.gov/castnet/tdep/Total_Deposition_Documentation_current.pdf (2022).
28. Turner, R. E. Declining bacteria, lead, and sulphate, and rising pH and oxygen in the lower Mississippi River. *Ambio* **50**, 1731–1738 (2021).
29. Census, U. No. HS-28. National Air Pollutant Emissions: 1900 to 2000. *Statistical Abstract of the United States* (2003).
30. EPA. *2020 National Emissions Inventory and Trends Report*. https://www.epa.gov/air-emissions-inventories/2020-national-emissions-inventory-nei-data (2020).
31. Cao, P., Lu, C. & Yu, Z. Historical nitrogen fertilizer use in agricultural ecosystems of the contiguous United States during 1850-2015: Application rate, timing, and fertilizer types. *Earth Syst Sci Data* **10**, 969–984 (2018).
32. Meng, C. *et al.* Global soil acidification impacts on belowground processes. *Environmental Research Letters* **14**, (2019).
33. Hamilton, S. K., Kurzman, A. L., Arango, C., Jin, L. & Robertson, G. P. Evidence for carbon sequestration by agricultural liming. *Global Biogeochem Cycles* **21**, 1–12 (2007).
34. Maxwell, R. M. *et al.* The imprint of climate and geology on the residence times of groundwater. *Geophys Res Lett* **43**, 701–708 (2016).
35. Reitz, M., Sanford, W. E., Senay, G. B. & Cazenas, J. Annual Estimates of Recharge, Quick-Flow Runoff, and Evapotranspiration for the Contiguous U.S. Using Empirical Regression Equations. *J Am Water Resour Assoc* **53**, 961–983 (2017).

36. Appelo, C. A. J. Cation and proton exchange, pH variations, and carbonate reactions in a freshening aquifer. *Water Resour Res* **30**, 2793–2805 (1994).
37. Spencer, W. F. Influence of cation-exchange reactions on retention and availability of cations in sandy soils. *Soil Sci* **77**, 129–136 (1954).
38. Bolt, G. H. & Bruggenwert, M. G. M. *Soil Chemistry. A. Basic Elements.* (1978).
39. Kanzaki, Y. *et al.* Soil cation storage is a key control on the carbon removal dynamics of enhanced weathering. *Environmental Research Letters* **20**, 1–11 (2025).
40. Wieczorek, M. E. Area- and Depth- Weighted Average of Soil pH from STATSGO2 for the Conterminous United States and District of Columbia. Preprint at https://doi.org/10.5066/P95YOSFQ (2019).
41. Levy, C. R. *et al.* Enhanced Rock Weathering for Carbon Removal − Monitoring and Mitigating Potential Environmental Impacts on Agricultural Land. *Environ Sci Technol* **58**, (2024).
42. Zhang, X. *et al.* Managing nitrogen for sustainable development. *Nature* **528**, 51–59 (2015).
43. USGS. National Water Information System data available on the World Wide Web (USGS Water Data for the Nation). http://waterdata.usgs.gov/nwis/ (2016) doi:10.5066/F7P55KJN.
44. Kanzaki, Y., Chiaravalloti, I., Zhang, S., Planavsky, N. J. & Reinhard, C. T. In silico calculation of soil pH by SCEPTER v1.0. *Geosci Model Dev* **17**, 4515–4532 (2024).
45. Kanzaki, Y., Zhang, S., Planavsky, N. J. & Reinhard, C. T. Soil Cycles of Elements simulator for Predicting TERrestrial regulation of greenhouse gases: SCEPTER v0.9. *Geosci Model Dev* **15**, 4959–4990 (2022).
46. Dole, R. B. *The Quality of Surface Waters in the United States*. *Water-Supply Paper 236* (US Government Printing Office, 1909).
47. Sewerage and Water Board (New Orleans, L. *Report on Water Purification Investigation and on Plans Proposed for Sewerage and Water-Works Systems*. (Hyatt, 1903).
48. Goolsby, D. a *et al. Flux and Sources of Nutrients in the Mississippi – Atchafalaya River Basin*. *National Ocean Service Coastal Ocean Program* (National Oceanic and Atmospheric Administration, 1999).
49. Gaillardet, J., Dupré, B., Louvat, P. & Allègre, C. J. Global silicate weathering and CO2 consumption rates deduced from the chemistry of large rivers. *Chem Geol* **159**, 3–30 (1999).
50. Kantzas, E. P. *et al.* Substantial carbon drawdown potential from enhanced rock weathering in the United Kingdom. *Nat Geosci* **15**, 382–389 (2022).
51. Khalil, K., Mary, B. & Renault, P. Nitrous oxide production by nitrification and denitrification in soil aggregates as affected by O2 concentration. *Soil Biol Biochem* **36**, 687–699 (2004).
52. Brady, N. C. & Weil, R. R. *The Nature and Properties of Soils*. (Pearson, 2016).
53. Nishina, K., Ito, A., Hanasaki, N. & Hayashi, S. Reconstruction of spatially detailed global map of NH4+ and NO3application in synthetic nitrogen fertilizer. *Earth Syst Sci Data* **9**, 149–162 (2017).
54. Lu, C. & Tian, H. Global nitrogen and phosphorus fertilizer use for agriculture production in the past half century: Shifted hot spots and nutrient imbalance. *Earth Syst Sci Data* **9**, 181–192 (2017).

55. Billen, G., Garnier, J. & Lassaletta, L. The nitrogen cascade from agricultural soils to the sea: Modelling nitrogen transfers at regional watershed and global scales. *Philosophical Transactions of the Royal Society B: Biological Sciences* **368**, (2013).
56. Milici, R. C. The COALPROD database: historical production data for the major coal-producing regions of the conterminous United States. in *U.S. Geological Survey 97-447A* (1997).
57. Raymond, P. A. & Oh, N. H. Long term changes of chemical weathering products in rivers heavily impacted from acid mine drainage: Insights on the impact of coal mining on regional and global carbon and sulfur budgets. *Earth Planet Sci Lett* **284**, 50–56 (2009).
58. Sharma, R. K., Cox, M. S., Oglesby, C. & Dhillon, J. S. Revisiting the role of sulfur in crop production: A narrative review. *J Agric Food Res* **15**, 101013 (2024).
59. Riley, N. G., Zhao, F. J. & McGrath, S. P. Leaching losses of sulphur from different forms of sulphur fertilizers: A field lysimeter study. *Soil Use Manag* **18**, 120–126 (2002).
60. Degryse, F., Baird, R., Andelkovic, I. & McLaughlin, M. J. Long-term fate of fertilizer sulfate- and elemental S in co-granulated fertilizers. *Nutr Cycl Agroecosyst* **120**, 31–48 (2021).
61. Smith, S. J. & Andres, R. *Historical Sulfur Dioxide Emissions 1850-2000: Methods and Results*. *No. PNNL-14537.* (Pacific Northwest National Lab.(PNNL), Richland, WA (United States), 2004).
62. Smith, S. J., Pitchera, H. & Wigley, T. M. L. Global and regional anthropogenic sulfur dioxide emissions. *Glob Planet Change* **29**, 99–119 (2001).
63. EPA. Nitrogen Dioxide/Nitrogen Oxide In-Stack Ratio (ISR) Database. *Environmental Protection Agency Support Center for Regulatory Atmospheric Modeling (SCRAM)* https://www.epa.gov/scram/nitrogen-dioxidenitrogen-oxide-stack-ratio-isr-database (2024).
64. Tuanmu, M. N. & Jetz, W. A global 1-km consensus land-cover product for biodiversity and ecosystem modelling. *Global Ecology and Biogeography* **23**, 1031–1045 (2014).
65. Fick, S. E. & Hijmans, R. J. WorldClim 2: new 1-km spatial resolution climate surfaces for global land areas. *International Journal of Climatology* **37**, 4302–4315 (2017).
66. Zhao, M., Heinsch, F. A., Nemani, R. R. & Running, S. W. Improvements of the MODIS terrestrial gross and net primary production global data set. *Remote Sens Environ* **95**, 164–176 (2005).
67. Poggio, L. *et al.* SoilGrids 2.0: Producing soil information for the globe with quantified spatial uncertainty. *Soil* **7**, 217–240 (2021).
68. Walkinshaw, M., O'Geen, A. T. & Beaudette, D. E. Soil Properties. *California Soil Resource Lab* https://play.google.com/store/apps/details?id=com.alfaandfriendssdnbhd.lsj&hl=en&gl=US&pli=1 (2023).
69. Zeng, S., Kaufmann, G. & Liu, Z. Natural and Anthropogenic Driving Forces of Carbonate Weathering and the Related Carbon Sink Flux: A Model Comparison Study at Global Scale. *Global Biogeochem Cycles* **36**, 1–21 (2022).
70. Renforth, P. & Henderson, G. Assessing ocean alkalinity for carbon sequestration. *Reviews of Geophysics* **55**, 636–674 (2017).
71. Turner, R. E. Total ammonia and coliform concentrations at the end of the Mississippi River from 1900 to 2019. *Environ Monit Assess* 1–6 (2023) doi:10.1007/s10661-022-10903-1.

72. Turner, R. E., Milan, C. S., Swenson, E. M. & Lee, J. M. Peak chlorophyll a concentrations in the lower Mississippi River from 1997 to 2018. 703–712 (2022) doi:10.1002/lno.12030.
73. Suhrhoff, T. J. *et al.* A tool for assessing the sensitivity of soil-based approaches for quantifying enhanced weathering: a US case study. *Frontiers in Climate* **6**, 1–17 (2024).
74. Smith, D. B. *et al.* Geochemical and mineralogical data for soils of the conterminous United States. *U.S. Geological Survey Data Series* **801**, 1–26 (2013).
75. Zamanian, K., Zarebanadkouki, M. & Kuzyakov, Y. Nitrogen fertilization raises CO2 efflux from inorganic carbon: A global assessment. *Glob Chang Biol* **24**, 2810–2817 (2018).
76. Hénault, C. *et al.* Management of soil pH promotes nitrous oxide reduction and thus mitigates soil emissions of this greenhouse gas. *Sci Rep* **9**, 1–11 (2019).
77. Blanc-Betes, E. *et al.* In silico assessment of the potential of basalt amendments to reduce N2O emissions from bioenergy crops. *GCB Bioenergy* **13**, 224–241 (2021).
78. Knapp, W. J. & Tipper, E. T. The efficacy of enhancing carbonate weathering for carbon dioxide sequestration. *Frontiers in Climate* **4**, 1–21 (2022).

supporting information

Acidity addition in the Mississippi watershed drives agricultural CO_2 emissions

Tim Jesper Suhrhoff[1,2*], Christopher T. Reinhard[3], Yoshiki Kanzaki[3], Shou-En Tsao[4], Beck Woollen[1], Tom Reershemius[2], James Saiers[4], Shuang Zhang[5], Peter A. Raymond[4], Noah J. Planavsky[2,1]

[1] Yale Center for Natural Carbon Capture, Yale University, New Haven, CT 06511, USA

[2] Department of Earth and Planetary Sciences, Yale University, New Haven, CT 06511, USA

[3] School of Earth & Atmospheric Sciences, Georgia Institute of Technology, Atlanta, GA 30332, USA

[4] Yale School of Forestry and Environmental Studies, Yale University, New Haven, CT 06511, USA

[5] Department of Oceanography, Texas A&M University, College Station, TX 77843, USA

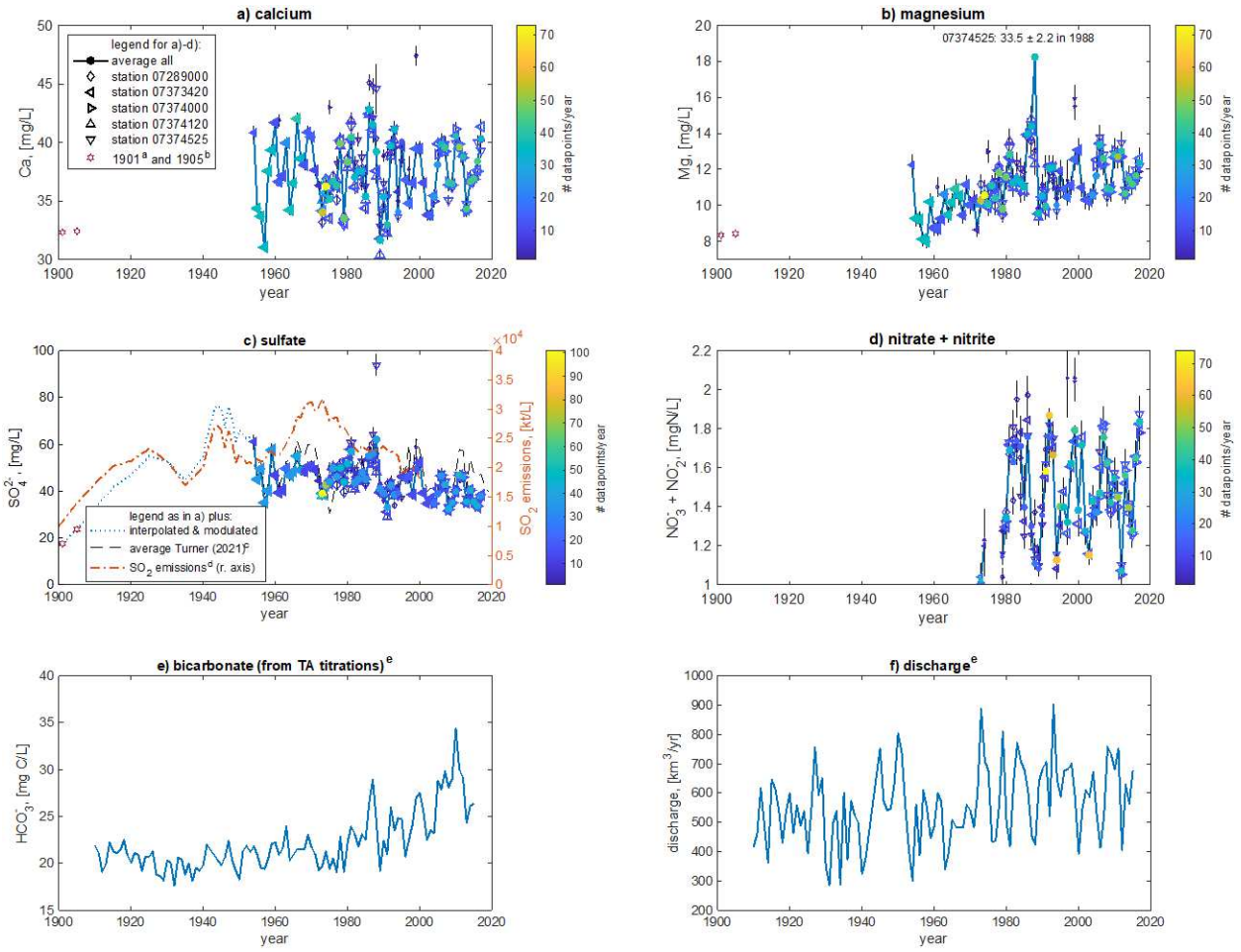
* corresponding author: timjesper.suhrhoff@yale.edu

S1 River chemistry records and extended discussion

In combination with published riverine alkalinity concentrations and water fluxes within the MRB[22,23], the data compiled here (**Figure S1**) can be used to investigate strong acid weathering. It is possible to assess the extent to which strong acids are involved in the dissolution of lime[33] by comparing the concentrations of Ca^{2+} and Mg^{2+} to HCO_3^- (in meq/L; **Figure S2**a, see also online methods including **Figure 4**). If Ca+Mg concentrations were the same as HCO_3^-, all lime dissolution would occur due to reaction with carbonic acid[33]. Typically, HCO_3^- concentrations are lower, with the difference representing either loss of bicarbonate because of reaction with strong acids (equation 12), or dissolution of lime with strong acids which produces Ca+Mg but not HCO_3^- (equation 13). The difference between these concentrations may be used to estimate the fraction of lime dissolution that has occurred because of strong acid weathering ($f_{strong\ acid}$) as well as the CO_2-sink strength. Both measures are related, with the latter expressing the CDR impact of lime relative to the amount of carbon the lime itself contains (see online methods).

Usually, this approach is applied to tile drainage and stream water[33]. Here, we assume that this framework also applies to the Mississippi watershed for three reasons. First, ~58% of the catchment is covered with croplands[48]. Hence, overall riverine processes are heavily impacted by agriculture [1,20–24], facilitating the emergence of an agricultural liming signal. Second, although on catchment scale not only carbonate but also silicate and evaporite weathering clearly impact dissolved loads, including K and Na in the analysis (reflecting these lithologies) does not impact the observed trend in cation vs. HCO_3^- space (compare **Figure S2a** and **Figure S6a**). Third, weathering fluxes in the Mississippi catchment are generally dominated by carbonate weathering[49], such that this framework would be expected to reflect carbonate weathering dynamics also on the catchment scale.

The reactions of strong acids with lime and bicarbonate (equations 11-13) can be visualized as vectors (vectors labeled 1-3 in **Figure S2**a), which allows us to qualitatively assess how the relative importance of the different reaction pathways has changed through time in the Mississippi watershed.



872

873 *Figure S1: Average annual concentration of Ca (a), Mg (b), SO_4^{2-} (c), NO_3^- + NO_2^- (d), HCO_3^- (e), and water discharge in the*
874 *Lower Mississippi River. Calcium concentrations (a) show large interannual variability with no discernible trend (although*
875 *discharge increases (f), suggesting an increase in annual fluxes. Magnesium concentrations (b) increase during the instrumental*
876 *record while SO_4^{2-} concentrations (c) decrease. For the gaps in the record, SO_4^{2-} concentrations are interpolated and modulated*
877 *by SO_2 emissions, suggesting increased concentrations in the 40s, while, bounded by data from 1901*[47] *and 1905*[46]*, concentrations*
878 *were low at the beginning of the 20th century. Nitrate and nitrite concentrations have a high variability with no discernible trend*
879 *(d). Bicarbonate concentrations*[22] *increase after 1980 (e), similarly to discharge (f) though the discharge signal has a lower signal*
880 *to noise ratio. Average flow-weighted concentrations in (a)-(d) are calculated from 5 USGS stations*[43] *in the Lower Mississippi*
881 *(see **Figure 1** for locations), the data for each station and the average are shown, with marker size being proportional to the*
882 *number months with data within a year, and the color corresponding to the datapoints within a given year. Uncertainties in a-d*
883 *are propagated assuming 5% uncertainty on concentration measurements and 10% uncertainty on discharge. When propagated*
884 *uncertainties were below 5%, a minimum of 5% was assumed for flow weighted uncertainties. Bicarbonate concentrations (e) are*
885 *derived from total alkalinity titrations, assuming that the majority of alkalinity is derived from HCO_3^-, and originate from the*
886 *Sewage and Water Board of New Orleans*[22,23]*. Estimates of annual Mississippi discharge are derived from long records of 84*
887 *USGS sites and contain discharge diverted into the Atchafalaya River*[23]*. Uncertainties on HCO_3^- and discharge are assumed to be*
888 *10%.*
889 *[a] Sewage and Water Board (New Orleans, LA) (1903)*[47] *[b] (Dole, 1909)*[46] *[c] Turner (2021)*[28] *[d]* based on data from Turner (2021) and
890 U.S. Bureau of Census[28–30] *[e] Raymond & Hamilton, 2018*[22]

891

892 Compared to the year 1900, changes in the composition of Mississippi River water suggest that
893 the reaction of carbonate rock with strong acids (either through reaction 13 or 11+12) dominates
894 the evolution of water chemistry up until ~1980. After 1980, the impact of strong acids has

decreased while cation concentrations stay similar (reduction in equation 12), which also causes $f_{strong\ acid}$ to decrease below 1900 levels after ~2000. Measured values for the fraction of strong acid weathering ($f_{strong\ acid}$) are between 30-40% (CO_2-sink strength of 20-40%) between 1954 and 1990 before they drop to ~20% (CO_2-sink strength of 60-80%; **Figure S2**), indicating that carbonate weathering has been a CO_2 sink throughout the whole period. In terms of CO_2-sinks strength, the values are consistent with measurements from agricultural streams for the pre-1990 period[33] before increasing to more pristine values, demonstrating evolution into a more CO_2-removing regime.

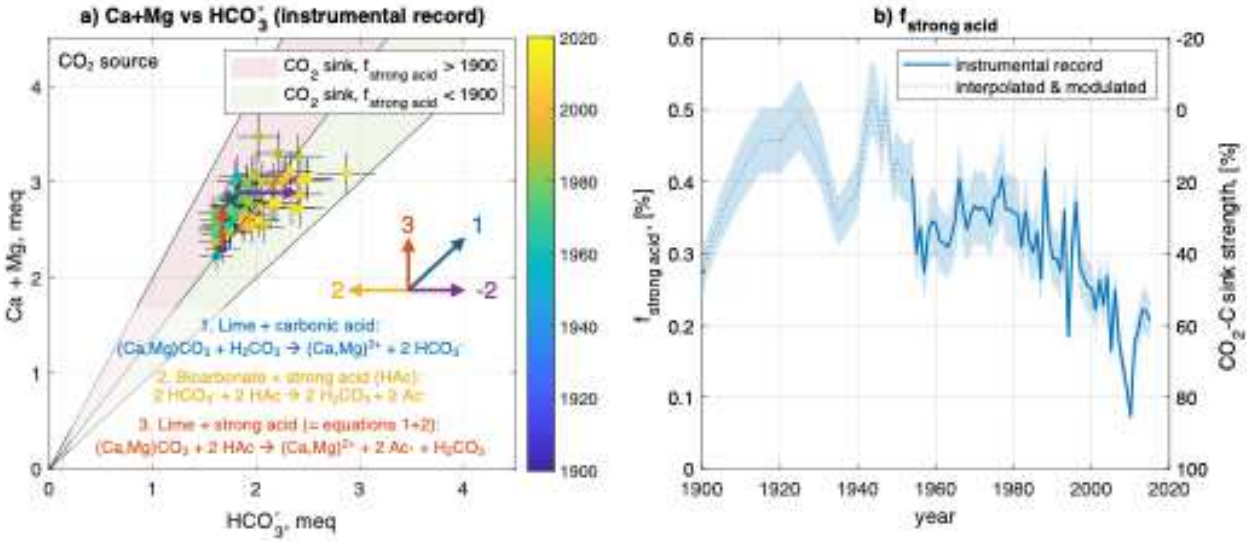
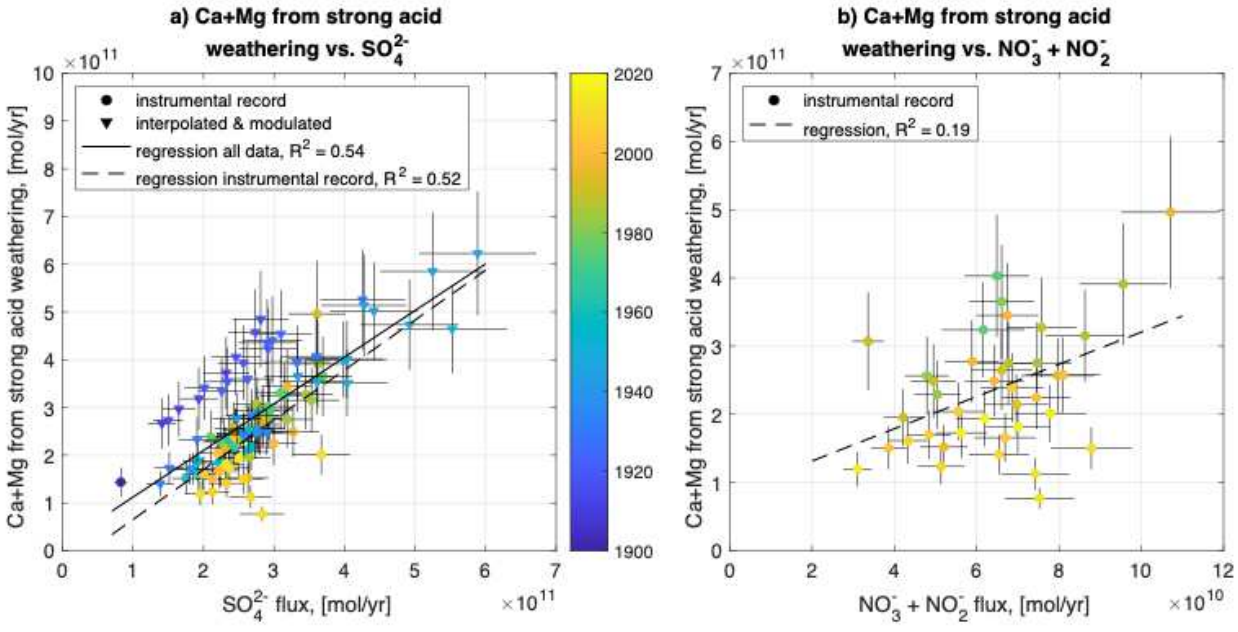


*Figure S2: Panel a) shows how Ca+Mg and HCO_3^- changed over time (corresponding to the marker color). The data from all years fall into the CO_2 sink area as defined by $[HCO_3^-] > 0.5 * [Ca+Mg]$ (in meq)[33]. The vectors shown in the panel a refer to the effect that the reactions displayed in the bottom have in [Ca+Mg] vs. $[HCO_3^-]$ space, with -2 being the effective trend imposed by a reduction in the extent to which reaction 2 occurs. The trend observed over time is consistent with an increase in Ca+Mg concentrations being driven by reactions of lime with strong acid (equation 3), and a reduction of strong acid weathering (reduction of reaction 2) at equal lime dissolution rates. As a result, before ~1980, the CO_2 sink strength was lower than in 1900, but has increased over 1900 levels since then (lower $f_{strong\ acid}$, panel b). Including K and Na in the analysis (reflecting silicate and evaporite weathering) does not impact the observed trend in cation vs. HCO_3^- space (compare **Figure S1**). Panel b) shows the $f_{strong\ acid}$ in the Lower Mississippi from 1900-2015. The fraction of strong acid for the post 1953 period is calculated based on the USGS cation data and published alkalinity/bicarbonate data[22,23]. Between 1901-1953, it is interpolated between measured data points in 1900 and 1954 and modulated by changes in SO_2 emissions[28–30] and acidity production from fertilizer oxidation (see methods). The fraction of strong acid is highest during the interpolated period. During the period constrained by instrumental records, the fraction strong acid is 30-40% between1954 and the 90s, when it starts dropping to below 20% in the years 2007-2012. CO_2-C sink strength[33] (right y-axis panel b) essentially refers to the fraction of C in lime that is a CO_2 sink (positive values) or CO_2 source (negative values; see online methods).*

Driven by both a lower fraction of strong acid weathering and larger overall weathering fluxes, on timescales shorter than carbonate precipitation in the oceans (>10kyr[70]), carbonate weathering is today a stronger CO_2 sink in the Mississippi river catchment than it was in 1900. The decrease in

924 $f_{strong\ acid}$ (and related increase in C-sink strength) is primarily driven by decreases in acidity input,
925 which is consistent with the decreased acidity input after 1970 (**Figure 2d**), the evolution in cation
926 vs. bicarbonate space (**Figure S2**a), and the fact that strong acid derived cation loads are correlated
927 with riverine strong acid anions, with both decreasing over time (particularly SO_4^{2-}; R^2=0.52,
928 **Figure S3**). At the same time, the increase in overall weathering flux is likely driven by the
929 increase in catchment wide liming starting in the late 1930s as the increase in cation fluxes is
930 consistent with the amount of cations contained in the lime added to the Mississippi watershed.
931 Post-1953 Ca+Mg concentrations are ~21% higher than the 1900 value. The post-1939 lime
932 addition corresponds to ~18 % riverine Ca+Mg fluxes over the same period (**Figure S4**).
933



934

935 *Figure S3: The flux of Ca+Mg driven by strong acid weathering (i.e., pseudo-cation flux * $f_{strong\ acid}$) has a high correlation with*
936 *riverine SO_4^{2-} fluxes (panel b), suggesting the observed changes may be driven by changes in sulfuric acid inputs. The correlation*
937 *with NO_3^-+NO2- is lower (R2 = 0.19, panel c), consistent with constant fertilizer oxidation at dropping $f_{strong\ acid}$.*

938

939 The decrease in strong acid addition and increase in liming also have combined effects. The
940 negative correlation between bicarbonate fluxes and $f_{strong\ acid}$ (**Figure S5**; R^2 = 0.38 for the
941 instrumental record) suggests that the increase in bicarbonate export (**Figure S1e**) may be, among
942 other factors[1,20–24,28,57,71,72], driven by reductions in CO_2 degassing due to lower acidity inputs.
943 Furthermore, although ultimately forced by acidity inputs, the decrease of $f_{strong\ acid}$ is also impacted
944 by lime addition simply because it increases both cation and bicarbonate fluxes, causing $f_{strong\ acid}$

to decrease. Collectively these strands of river-chemistry-based evidence are consistent with the notion that acidity addition drives CO_2 emissions, and that liming can be considered a CO_2 sink.

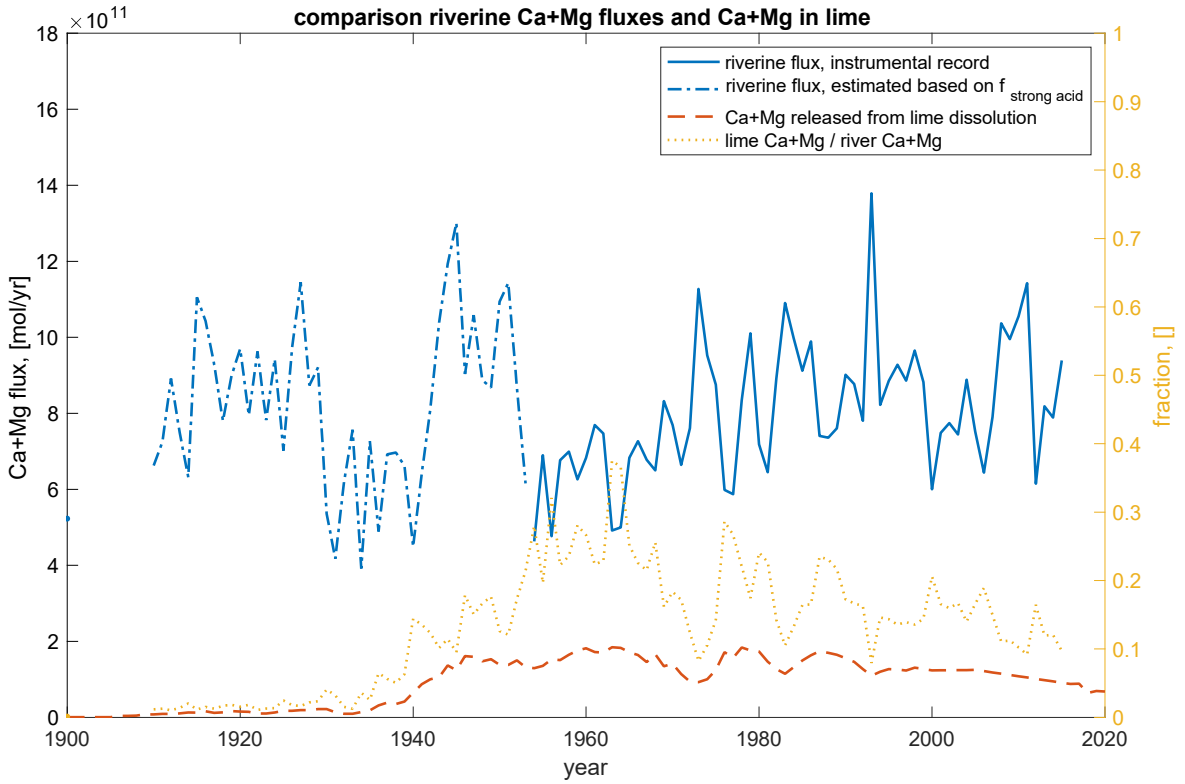


Figure S4: This figure compares riverine fluxes of Ca and Mg (blue) to the amount of Ca added in fields (orange), with the ratio of the latter to the former shown in yellow (right axis). The average post-1939 ratio is ~0.18. Note that the shown riverine Ca+Mg flux is a combination of the instrumental record (solid line) and an estimation based on riverine HCO_3^- fluxes as well as the interpolated and modulated $f_{strong\ acid}$ (dashed-dotted line):

$$[Ca + Mg]_{pseudo} = \frac{[HCO_3^-]}{(1 - f_{strong\ acid})}$$

*Essentially, this approach is equivalent with correcting measured HCO_3^- concentrations to fall back on a 1:1 relationship between alkalinity generation and cation release from lime dissolution (on a charge basis). Graphically, this can be visualized by projecting HCO_3^- concentrations onto the 1:1 line in Ca+Mg vs. HCO_3^- space (**Figure 4**; **Figure S2**). These calculated "pseudo" cation concentrations are hence based on measured alkalinity and constraints on the fraction of lime that dissolves by reacting with strong acids. Given that they are based on the modulated $f_{strong\ acid}$, the data for this period has inherently larger scenario uncertainties based on the assumptions on the interpolation and modulation. In particular the large pulse in the 1940s is likely an artifact of the combined large river discharge (**Figure S1f**) as well as pulse in SO_2 emissions which feeds into the modulation of $f_{strong\ acid}$. The analysis presented here (comparison of Ca+Mg fluxes), however, this does not have an impact on the estimated ratio of Ca+Mg fluxes in lime as well as riverine records; using just the data from the instrumental record yields the same average ratio (~0.18).*

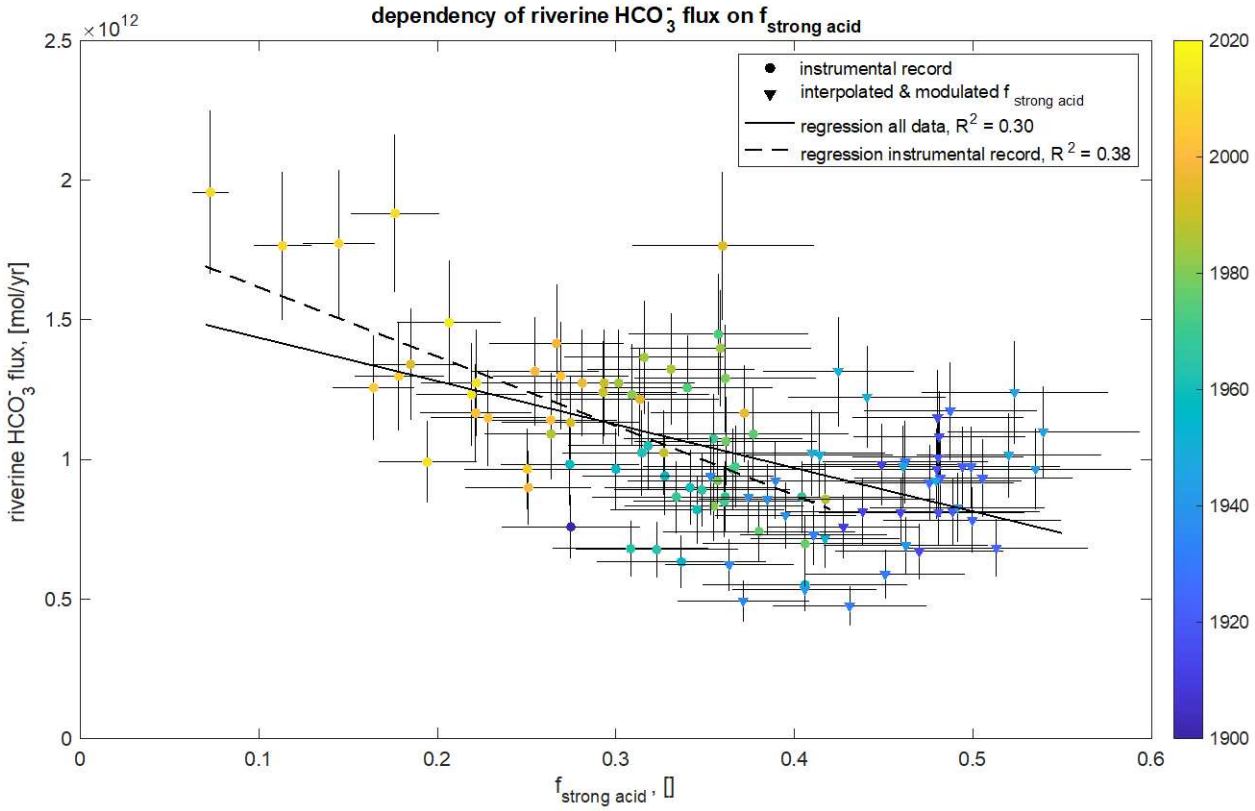


Figure S5: Riverine bicarbonate fluxes are negatively correlated with $f_{strong\ acid}$, which may indicate that at higher $f_{strong\ acid}$ some of the HCO_3^- is degassing as a result of reaction with H^+ derived from strong acids. Data based on the instrumental record is for the year 1900 as well as post-1953, while the period in between is based on the interpolated and modulate estimate of $f_{strong\ acid}$, which modulates $f_{strong\ acid}$ based on changes in acidity pollution in that time period.

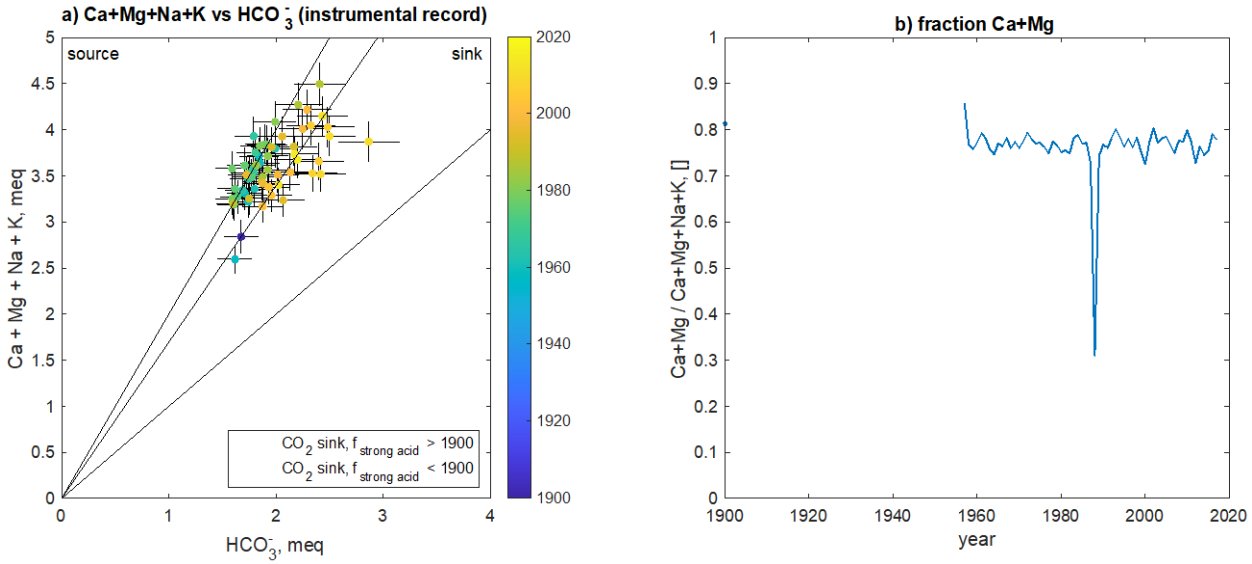


*Figure S6: Panel (a) shows major cations vs. bicarbonate concentrations (in meq/L). Such plots but based only on Ca+Mg are commonly used to gauge the fraction of strong acid weathering or the carbon sink strength of lime dissolution[33], which is shown in **Figure S2**. The version shown in panel (a) in addition also includes K+Na concentrations on the y-axis, demonstrating that the overall trends are equivalent in terms of an initial increase of cation concentrations followed by a recovery of HCO_3^- concentrations due to decreases in acidity pollution (**Figure S2a**). Because the sum of Ca+Mg+Na+K is by definition higher than the sum of Ca+Mg, values are shifted to higher y-axis values, i.e., higher $f_{strong\ acid}$ and lower carbon sink strength (it is a stronger relative C source compared to just using Ca+Mg). Panel (b) shows the fraction of Ca+Mg relative to Ca+Mg+Na+K (in meq/L), which has stayed constant from 1960 to 2016 at ~0.775, likely because overall weathering fluxes are dominated by carbonate weathering anyways[49] and/or due to buffering of released cations via the cation exchange pool. The low value in 1988 is the result of anomalously high Na concentrations. These high concentrations were only observed at station 07374525, and not at stations 07373420 and 07289000 which also have data in this year (although less datapoints) and is therefore likely the result of local pollution.*

S2 Acidity as a driver for CO_2 emissions from agriculture

Dissolution reactions with limestone in soil consume acidity—depending on soil conditions, the predominant acids in this reaction are either carbonic acid (above a pH of 5-6[17]) or stronger acids such as nitric or sulfuric acid[1,33]. With carbonic acid (H_2CO_3), limestone/dolomite ($(Ca,Mg)CO_3$) reacts to produce bicarbonate (HCO_3^-) and dissolved Ca and Mg. In the presence of protons from strong acids (HAc; Ac is a strong acid anion), bicarbonate neutralizes acidity and produces carbonic acid. Increasing carbonic acid concentrations drives CO_2 degassing:

$$(Ca,Mg)CO_3 + H_2CO_3 \rightarrow (Ca,Mg)^{2+} + 2\,HCO_3^- \quad \text{(eq. 11)}$$

$$2HCO_3^- + 2\,HAc \rightarrow 2\,H_2CO_3 + 2Ac^- \leftrightarrow 2CO_2 + 2\,H_2O + 2\,Ac^- \quad \text{(eq. 12)}$$

Alternatively, limestone in soils can react with strong acids directly to produce dissolved Ca and Mg, with charge balance maintained by the strong acid anion and loss of CO_2 through the equilibration of the carbonate system:

$$(Ca,Mg)CO_3 + 2\,HAc \rightarrow (Ca,Mg)^{2+} + 2\,Ac^- + H_2CO_3 \leftrightarrow (Ca,Mg)^{2+} + 2\,Ac^- + CO_2 + H_2O \quad \text{(eq. 13)}$$

This reaction is the basis for the conventional assumption that agricultural liming is a CO_2 source. For instance, in the current IPCC classification it is assumed that all the carbon contained in lime is emitted to the atmosphere. Based on contrasting findings on the CO_2 balance of liming[1,4,33], in US national GHG reporting it is assumed that only ~half of the C contained in carbonate soil amendment is emitted as CO_2.

Tying CO_2 emissions to lime addition is a mechanistically deficient framework for quantifying the processes controlling CO_2 fluxes. Linking emissions to lime addition confuses cause and effect—it is the reaction of acidity with bicarbonate that leads to CO_2 emissions[1], not the dissolution of limestone itself. Indeed, in the absence of strong acids liming would not release CO_2 and would instead straightforwardly lead to carbon dioxide removal (CDR). Furthermore, the conventional framework is also based on a flawed counterfactual, because it assumes that no liming would

equate to no CO_2 emissions. However, because there are natural alkalinity pools at Earth's surface (naturally occurring carbonates[73,74], bicarbonate in pore waters), anthropogenic acid inputs always lead to CO_2 emissions even in the absence of lime[75]. Further, if acidity input is larger than the alkalinity supplied by liming, the conventional framework will underestimate actual CO_2 emissions by failing to account for emissions occurring through the reaction of anthropogenic acids with natural pools of alkalinity. As a result, the current framework creates a flawed incentive structure. Real emission reductions could be achieved by lower acidity inputs through managing NO_x and SO_2 emissions as well as efficient use of fertilizer, but are not incentivized. Instead, management of soil pH through lime is penalized, removing a key tool farmers and land use planners can use to reduce agricultural emissions and improve soil health. Critically, elevating soil pH through liming decreases N_2O emissions[4,10,76] and increases nitrogen use efficiency (NUE)[4,10,76,77], reducing the need for nitrogen fertilizer and associated emissions from fertilizer production and nitrification.

Here, we propose a new framework for accounting for acid-base reactions in agricultural settings. We argue that quantification of CO_2 emissions should be tied to the addition of anthropogenic acidity, and that agricultural liming should be considered a CO_2 sink. We apply this framework to the MRB as a case study and demonstrate that it is consistent with both trends in river chemistry since 1900 as well as spatially-explicit reactive transport model simulations of soil CO_2 emissions resulting from inputs of acidity and alkalinity.

S3 Reactive transport model (SCEPTER)

As mentioned in the main text and online methods, SPECTER is spun up for 1°x1°C grid cells for the US where cropland constitutes at least 10% of areal extent[64] considering a soil depth of 0.5m. The initial and spin-up boundary conditions for the reactive transport code are based on a variety of gridded data products, including runoff/infiltration[35], mean annual air temperature[65], aboveground net primary productivity (NPP)[66], soil organic matter (SOM)[67], topsoil pH[67], soil cation exchange capacity (CEC)[68], and soil base saturation[67]. SCEPTER is initialized by tuning four key parameters:

5. a reference soil cation exchange coefficient ($K_{H/Na}$)[64]
6. dissolved Ca^{2+} concentration at the upper boundary, representing carbonate weathering and agricultural liming
7. input of soil organic carbon (J_{org})
8. soil organic carbon (SOC) turnover time (τ_{org}).

These parameters are adjusted to reproduce four site-specific observational parameters: soil pH, soil base saturation, soil organic carbon content, and soil pCO_2, which is estimated from soil temperature and net primary productivity[69]. The model is forced by other boundary conditions, such as runoff and air temperature. Before start of the simulations, the model is spun up for 10^5 yr to ensure processes are initially at steady state.

We transfer the acidity and alkalinity fluxes into the Mississippi River catchment (**Figure 2**) into corresponding mass fluxes for each grid cell (**Figure S7**). The fraction of nitrogen pollution that remains as acidity pollution (i.e., leaches from soils, see online methods and **Figure S11**) from both fertilizer and atmospheric pollution is fed into the system as NH_4NO_3 – essentially the compound does not affect the system trend as for both NH_4NO_3 and HNO_3, 1 mol of acidity is released per mol of N. Lime is introduced in the model as a 80:20 (by alkalinity) mix of $CaCO_3$ and dolomite $CaMg(CO_3)_2$. SO_2 pollution is inserted into the model domain as H_2SO_4.

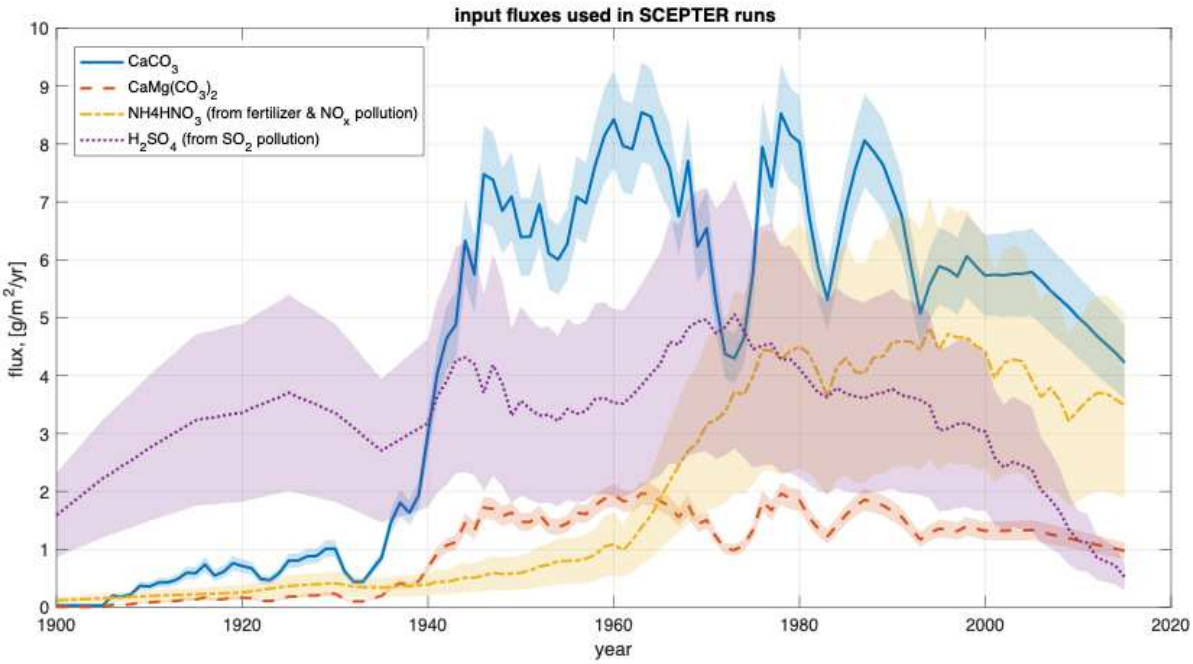


Figure S7: Input fluxes of lime and acidity generating compounds considered in the reactive transport code SCEPTER.

We suppress carbonate precipitations in the SCEPTER runs because (1) overall acidity inputs are larger than alkalinity inputs (main text **Figure 2**), making precipitation of secondary carbonates unlikely from a geochemical perspective, (2) there is considerable uncertainty for the threshold oversaturation required for such precipitation to occur[78].

Example outputs of spatially explicit model outputs are shown in **Figure S8**, where $f_{H,rxn}$ and $f_{H,diff}$ two different approaches to estimate the fraction of added acidity that reacts with bicarbonate to produce CO_2 emissions (see online methods). As the model output demonstrates, both approaches yield similar estimates both in terms of spatial distributions and absolute values. We calculate the Mississippi average for these parameters as well as others to facilitate discussion at a catchment level (**Figure S9**).

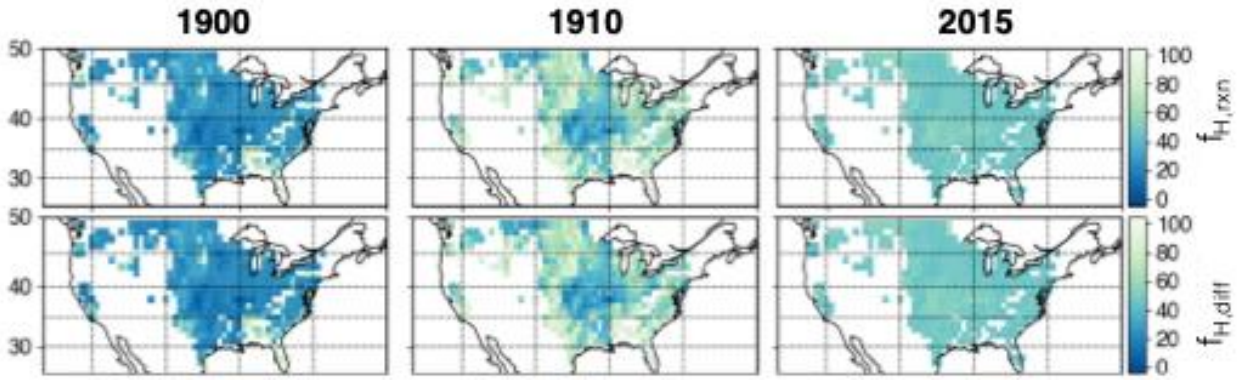


Figure S8: Input fluxes of lime and acidity generating compounds considered in the reactive transport code SCEPTER.

The temporal dynamics of acidiy fluxes to and from the cation exchange complex (CEC) pool as well as reacting with bicarbonate are complex and depend on land use history (**Figure S9**). In the beginning of the record, acidity addition is larger than alkalinity addition with liming being essentially absent (**Figure 2**). In this part of the record the CEC complex is an acidity sink, with protons exchanging on CEC for base cations. When liming increases in the 1930s, releasing base cations in top soils and reducing acidity-alkalinity imbalance, the CEC complex becomes an acidity source as cations exchange with protons on CEC sites, increasing base saturation. This process oscillates between CEC being an acid sink and source over time depending on how the balance between acidity and alkalinity addition develops in a certain year. The seeming imbalance in the mass balance in **Figure S9**a (more sources than sinks plotted) after ~1930 results from the reaction of acidity with lime, which is an additional acidity sink and not shown.

Because the CEC complex saturates with acidity in the beginning of the record, progressively less protons are sorbed to CEC sites and more reacts with bicarbonate to produce CO_2, causing a continuous increase in the CO_2 emissions flux until 1940. After this the dynamics become more complex with acidity from direct pollution as well as the CEC complex and the input of lime as an additional CO_2 sink all modulating this flux.

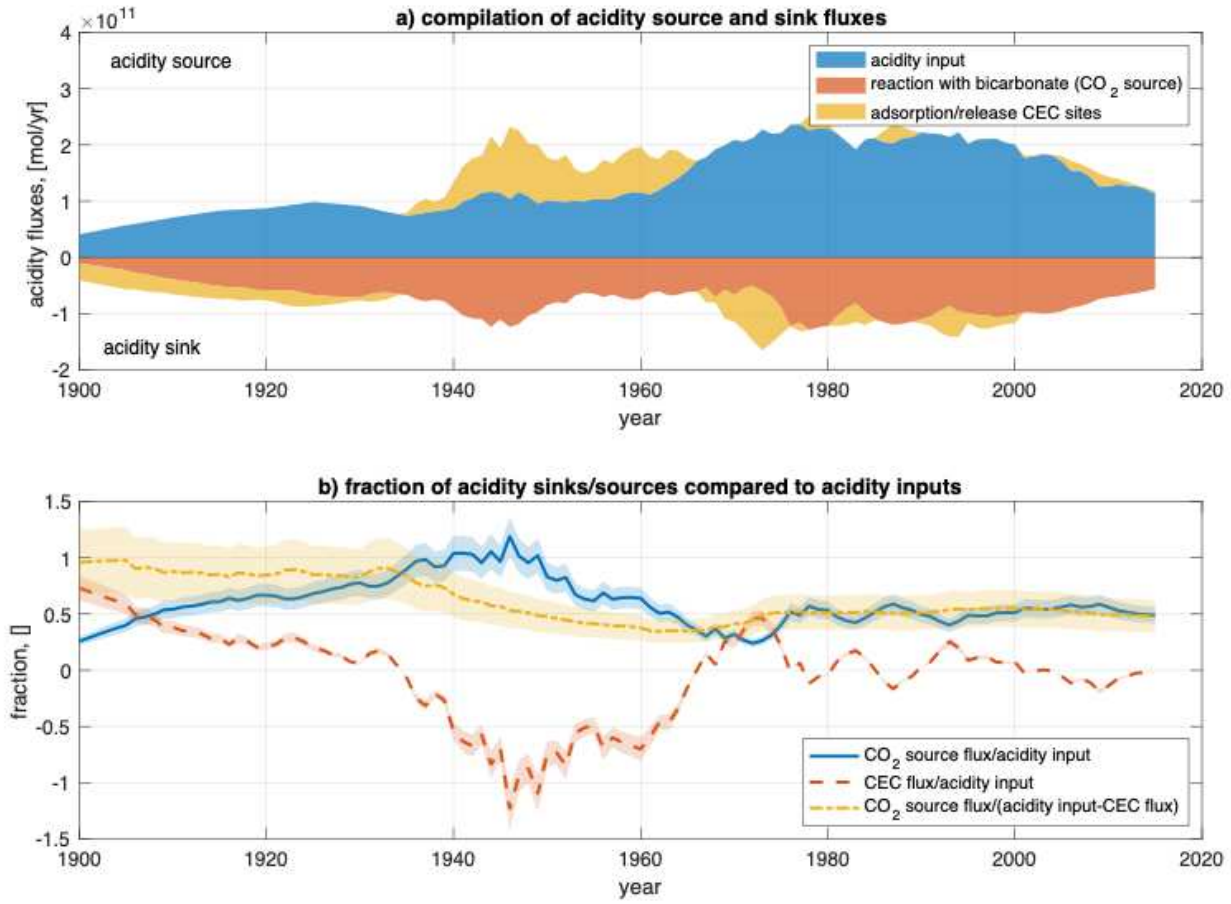


Figure S9: Panel a) shows sources and sinks of acidity within the soil column considered in SCEPTER, with negative values corresponding to acidity sinks and positive values as acidity sources. The cation exchange (CEC) pool acts both as a CO_2 source and CO_2 sink depending on the relative inputs of acidity and cations in a given year. Panel b) shows the flux of acidity reacting with bicarbonate to produce CO_2 relative to the input of acidity from pollution (blue line) and relative to the net acidity input also accounting for fluxes from the CEC complex (yellow dash-dotted line). The acidity flux to/from the CEC complex relative to acidity inputs from pollution is shown in orange (dashed line)

The relative fractions of the CO_2 flux normalized to acid input (**Figure S9b**) are used to calculate acidity-based CO_2 budgets based on acidity input into the soil column. The flux of acidity reacting with bicarbonate to produce CO_2 normalized by the net acidity addition (i.e., acidity pollution accounting for the flux to/from the CEC pool) starts of around 1 in the early part of the record before oscillating around 0.5 after 1960. Most acidity not adsorbing to CEC sites react to produce CO_2 (ratio close to 1). As liming increases in the 1930s, this value drops because the reaction of lime with protons is an additional acidity sink that emits CO_2 only at a 1:2 molar ratio (2 H^+ required for 1 mol of CO_2 emissions, see equation 3 in the main text).

S4 Additional supplementary figures main text & online methods

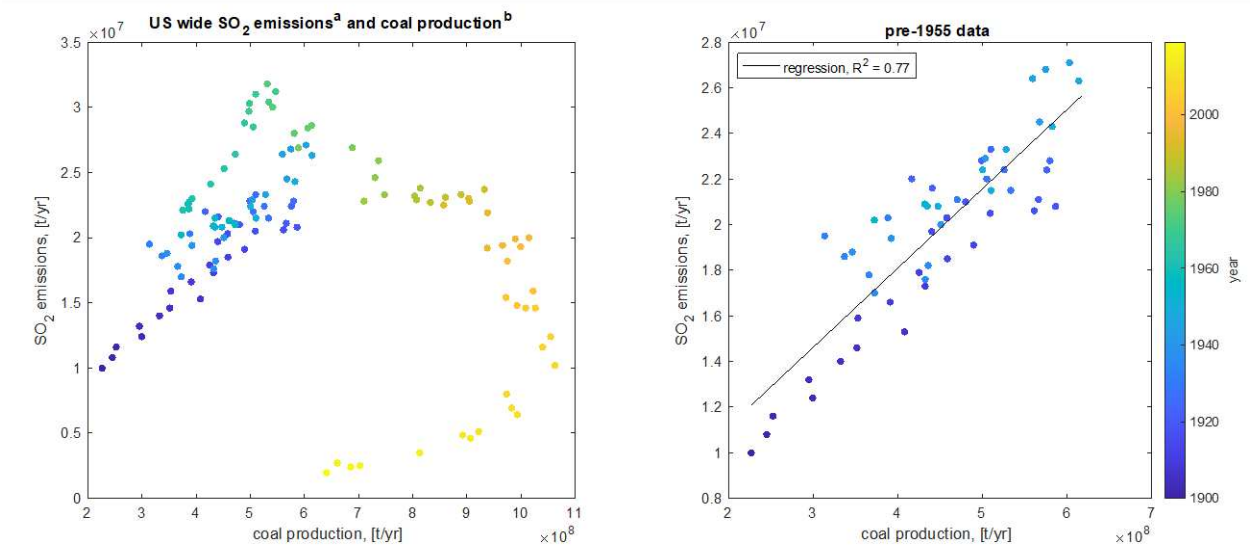


Figure S10: Panel (a) shows how SO_2 emissions and coal production have changed since 1900, and panel (b) shows the correlation between both parameters for the pre-1955 period where the SO_2 data was used to modulate $f_{strong\ acid}$ to demonstrate that to a large extent, in that period, dynamics in SO_2 emissions reflect changes in coal production. After this period SO_2 emissions decreased although coal production still increased (a), likely due to switching to coal with lower S content as well as the advent of industrial flu gas desulfurization technologies (1970 clean air act). After ~2000, both coal production and SO_2 emissions have decreased, following a new regression line with a lower slope (i.e., less SO_2 emissions at same coal production).

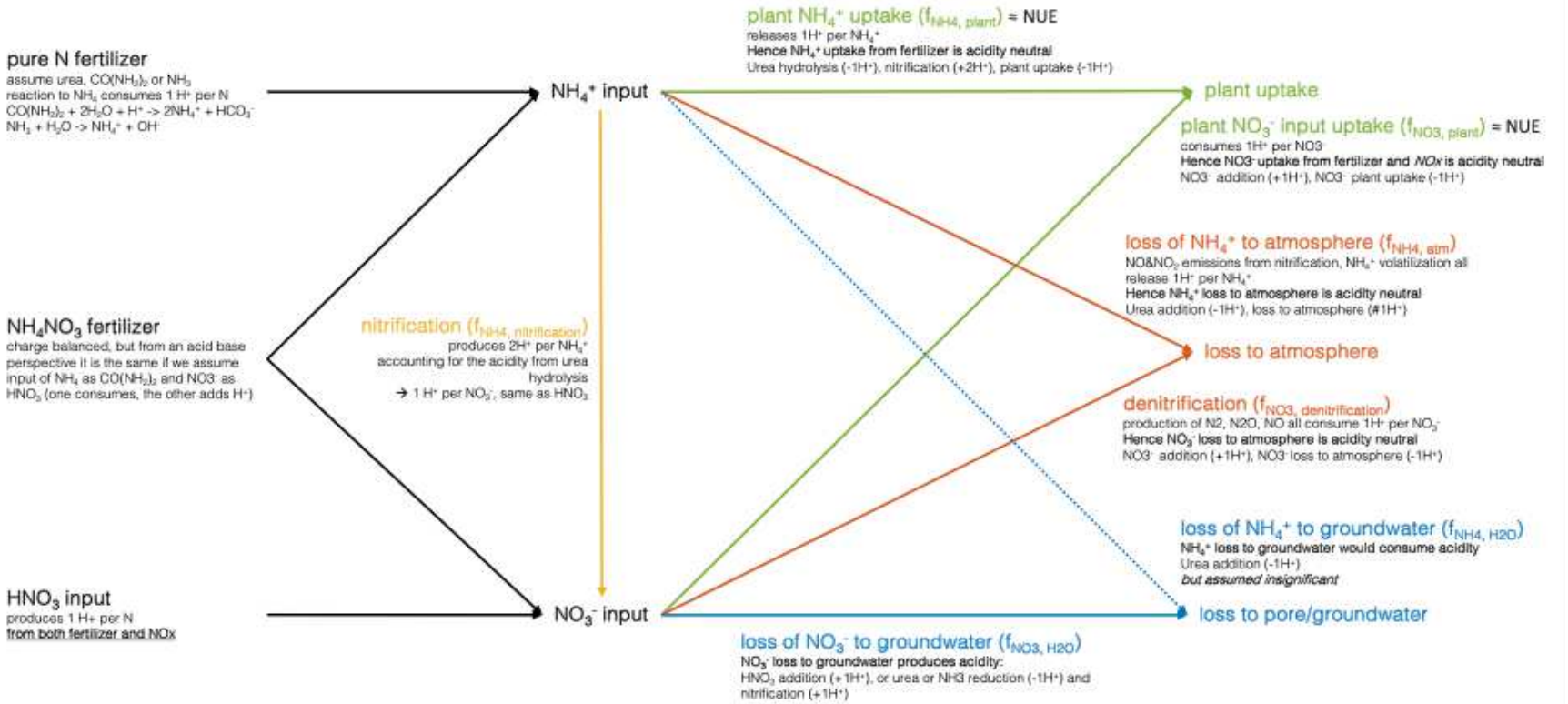


Figure S11: Sketch of the N cycle processes considered in this study. The assumptions laying the foundation for the analysis are that (1) irrespective of input type, N addition will release 1 mol H^+ per mol N, (2) that only the N remaining in porewaters and ultimately leached stays charge balanced with protons, with the rest of the processes being net-neutral in terms of acidity, and that the reaction of NH_4 to NO_3^- (nitrification) is assumed to dominate over plant uptake and groundwater losses, and losses to the atmosphere.

1) *All inputs of reduced N like urea ($CO(NH_2)_2$) or anhydrous ammonium (NH_3) consume 1 mol H^+ per mol N added to react to ammonia. Nitrification to NO_3^- produces 2 mol H^+ per mol ammonia, causing a net acidity input of 1 mol H^+ per mol N. Addition of HNO_3 deprotonates to 1 mol H^+ per mol N. Ammonium nitrate fertilizer (NH_4NO_3) is charge balanced without involving protons, but when the NH_4 is undergoing nitrification it produces 2 mol H^+ per mol N for 2 mol of N added. Hence for all of the most common N input types, the assumption of 1 mol H^+ per mol N added is valid.*

2) *Both plant uptake pathways as well as loss to the atmosphere neutralize the initial addition of acidity either directly through compensating fluxes of protons. As examples production of N_2, N_2O, and NO during denitrification all consume 1H^+ per NO_3^-. Similarly, production of NO and NO_2 from nitrification and NH_4^+ volatilization all consume 1 H^+ per mol N, at which point the process is acidity neutral as production of NH_4 consumes one proton per N. Plant uptake is either acidity balanced by direct fluxes of protons, or assumed to balance through charge balance and re-equilibration of the carbonate system.*

3) *In the simplified N-cycle calculations, we assume that NH_4 is quantitatively nitrified to NO_3^-, and that the plant uptake fraction of NO_3^- is approximated by the nutrient use efficiency (NUE), with the remainder being split between denitrification and leaching.*

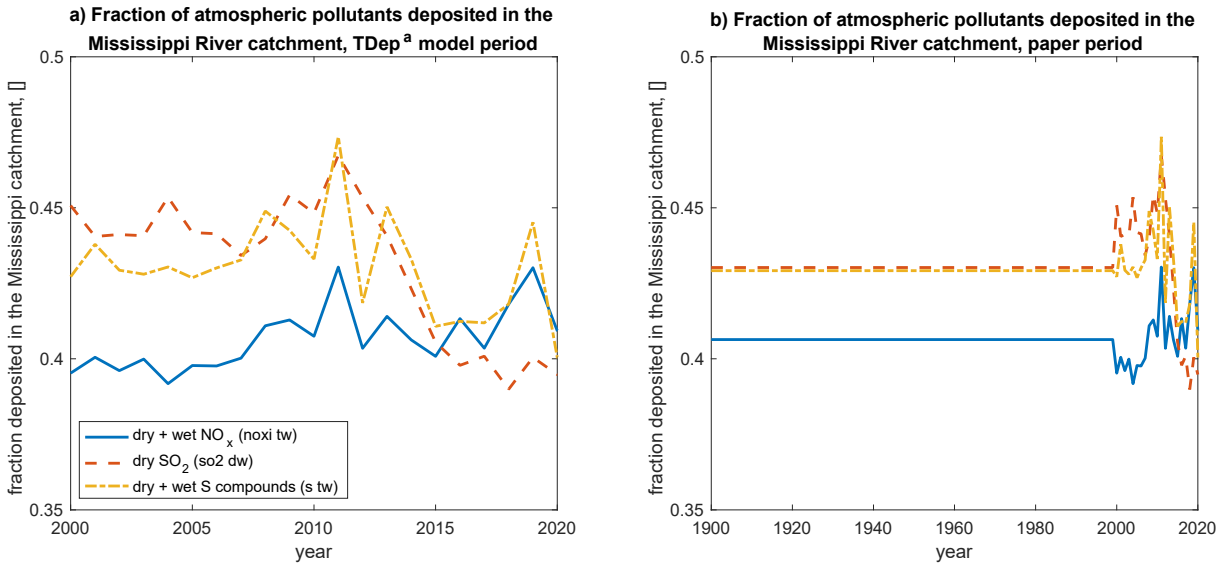


Figure S12: Fraction of US-wide atmospheric deposition of NOx and SO_2 in the Mississippi river catchment. The average of the years 2000-2021 is used to for the calculations from 1900-1999; assuming larger uncertainties for this period.